The impact of a central black hole on the hydrodynamic evolution of the gas injected within super stellar clusters

by

Filiberto Hueyotl Zahuantitla

A disertation submited to the Astrophysics
Department
in partial fullfilment of the requirements for the
degree of

MASTER OF SCIENCE

ASTROPHYSICS

at the

Instituto Nacional de Astrofísica, Óptica y Electrónica
August, 2007
Tonantzintla, Puebla

Advisors:

Dr. Sergiy Silich, INAOE
Dr. Guillermo Tenorio Tagle, INAOE

The impact of a central black hole on the hydrodynamic evolution of the gas injected within super stellar clusters

by

Filiberto Hueyotl Zahuantitla

A Dissertation
Submitted to the Program in Astrophysics,
Astrophysics Department

in partial fulfillment of the requirements for the degree of

MASTER OF SCIENCE
at the
Instituto Nacional de Astrofísica, Óptica y Electrónica
Tonantzintla, Puebla
Advisors:
Dr. Sergiy Silich
Dr. Guillermo Tenorio Tagle
INAOE

Abstract

We present the solution of spherically symmetric flows for the gas injected by stellar winds and supernova explosions within a super star cluster with a massive black hole at the center by using a self-consistent hydrodynamical model . We proof that our model always produce a stationary, self-consisten solution for the accretion flow and the star cluster wind, for any mass of the black hole. Although, the black hole does not modifies the large scale outflow, it shifts the threshold mechanical luminosity of the clusters to lower values. We demonstrate that in the case of star clusters with a central massive black hole the threshold mechanical luminosity separates clusters for which the stagnation radius and mass accretion rate are defined by the black hole from that, whose inner structure is defined by radiative cooling. We propose also an analytic approach to the numerical results, finding expressions for the mass accretion rate and the stagnation radius by using Bondi's accretion theory and the theory of adiabatic star cluster winds.

Resumen

Presentamos la solución de flujos esféricamente simétricos para el gas reinsertado por vientos estelares y explosiones de supernova dentro de un super cúmulo estelar con un agujero negro masivo central utilizando un modelo hidrodinámico autoconsistente. Probamos que nuestro modelo siempre produce una solución estacionaria, autoconsistente para el flujo de acreción y el viento del cúmulo para cualquier masa del agujero negro. Si bien el agujero negro no modifica la estructura a gran escala del viento, éste desplaza la luminosidad mecánica crítica de los cumulos hacia valores menores. Demostramos que en el caso de cúmulos estelares con un agujero negro masivo central la luminosidad mecánica crítica separa cúmulos para los cuales el radio de estancamiento y la tasa de acreción de masa son definidos por el agujero negro de aquellos, cuya estructura interna está definida por enfriamientoradiativo. También proponemos una aproximación analítica a los resultados numéricos encontrando expresiones para la tasa de acreción de materia y para el radio de estancamiento usando la teoría de acreción de Bondi y la teoría de vientos de cúmulos estelares en el caso adiabático.

Acknowledgements

I would like to express my deep-felt gratitude to my advisors, Dr. Sergiy Silich and Dr. Guillermo Tenorio Tagle of the Instituto Nacional de Astrofísica, Óptica y Electrónica (INAOE), Puebla, Méx., for their advice, encouragement, enduring patience and constant support. They were never ceasing in their belief in me (though I was often doubting in my own abilities), always providing clear explanations when I was (hopelessly) lost, constantly driving me with energy when I was tired, and always, *always* giving me their time, in spite of anything else that was going on.

I also thank to CONACyT for the financial support by the master grant 12442. Additionally, I want to thank the INAOE Astrophysics Department professors and staff for all their hard work and dedication, providing me the means to complete my degree.

Contents

Chapter 1

Introduction

Intensive studies of active galactic nuclei (AGNs) in optic, infrared (IR) and X-ray regimes during the last decade provided strong evidence for the presence of a massive starbursts around the central supermassive black hole (BH) in a number of Seyfert galaxies. In particular Heckman et al. (1997) and González Delgado et al. (1998) presented a direct evidence for the existence of nuclear starbursts in the four Seyfert 2 galaxies Mrk 477, NGC 7130, NGC 5135 and IC 3639. They found in the ultraviolet and optical spectra of these galaxies the absorption line features associated with photospheres of O and B stars and their stellar winds. The nuclear starbursts in these galaxies have sizes from less than 100 pc to a few hundred parsecs.

On the other hand, the strong correlation between the black hole mass and the velocity dispersion, $M_{BH}-\sigma$, (Ferrarese & Merritt 2000; Gebhardt et al. 2000; Merritt & Ferrarrese 2001; Tremaine et al. 2002; Greene & Ho 2006) or the black hole mass - bulge mass relation, $M_{BH}-M_{Bulge}$, (Merritt & Ferarrese 2001; Marconi & Hunt 2003; Häring & Rix 2004) in systems such as composite active galactic nuclei and non-active galaxies, indicates a tight connection between the central super-massive black hole and the surrounding spheroid or stellar cluster. This also led to the proposal that massive stellar clusters, like globular clusters, may host intermediate-mass black holes (Barth et al. 2005; Gebhardt et al. 2005; Greene & Ho 2006).

The synchronized activity of massive stars and supernovae within young stellar clusters results in a large scale outflow known as super wind or star cluster wind. The theory of star cluster winds has been studied extensively under the adiabatic approximation (Chevalier & Clegg 1985; Cantó et al. 2000; Raga et al. 2001), and in the more realistic radiative regime (Silich et al. 2004 and Tenorio-Tagle et al. 2007). However, so far there remains an open problem. How does the presence of a central black hole affect the hydrodynamics of the matter reinserted by the massive members of young stellar clusters? This problem was the motivation of the present dissertation.

1.1 The aim of this thesis

The goal of this thesis is to determine the impact of the gravity provided by a star cluster and by a central massive black hole on the hydrodynamic evolution of the gaseous outflows which result from the individual stellar winds and supernova explosions that occur within the cluster.

For this purpose, we develop a self consistent, spherically symmetric hydrodynamic model which takes into account radiative losses of energy and also the gravitational pull from the stellar component and that of the central black hole.

In order to understand how the gravitational field modifies the hydrodynamic structure of the flow inside the star cluster, in Chapter 2 we develop the isothermal solution for a star cluster wind in the two cases: with and without the gravitational pull of the cluster (see sections 2.2 and 2.3, respectively). In section 2.4 we discuss the isothermal assumption and in section 2.5 summarize our conclusions. Certainly, the isothermal assumption is far from reality. Nevertheless, this chapter allows us to understand how the hydrodynamics of star cluster winds are modified when gravity is added and also gives us the tools to handle more sophisticated models. In Chapter 3 we study the impact of the star cluster gravity on the radiative star cluster wind model developed by Silich et al. (2004). In section 3.2 we collect the basic equations associated with the adiabatic model of star cluster winds. In section 3.3 the solution of the basic equations including gravity terms is analyzed. In section 3.4 we formulate our main conclusions. In particular, in this chapter we demonstrate that the injected matter is accelerated more rapidly in more compact star clusters, despite the large gravitational force. We also demonstrate that the star cluster gravity does not significantly affect the shape of the integral curves found in Silich et al. (2004). In Chapter 4 we numerically solve the Bondi accretion problem in order to understand how a central black hole modifies the hydrodynamics of the gas inside the star cluster. In section 4.2 we introduce the physical restrictions of the model and the main equations for spherically symmetric accretion. In section 4.3 we present our method to solve the accretion problem and analyze the structure of the resulting flow for objects of different scales. In particular, in section 4.4 we apply our scheme to the M87 galaxy. Section 4.5 summarizes our conclusions. In this chapter we also prove that there is only one transonic solution for the spherically symmetric accretion problem. Although Bondi's theory uses a simplified polytropic gas law and does not take into consideration radiative losses of energy as well as the mass supplied by the star cluster, it is a useful reference to compare with the self-consistent theory developed in Chapter 5.

Chapter 5 is central in our study. Here we develop a self-consistent theory for an spherically symmetric accretion that takes into consideration radiative losses of energy, the mass deposition provided by the host stellar cluster and the gravitational field of the central massive black hole. In section 5.2 we discuss the input physics. In section 5.3 we introduce the main hydrodynamic equations and select the appropriate boundary conditions. There, we also discuss the family of integral curves that result from the selection of different stagnation radii. In section 5.4 we apply our model to the earlier stages of evolution of some galaxies and to star clusters with central black holes, whose parameters were taken from the literature. In this section we also propose an analytic approximation to the accretion rate and to the position of the stagnation radius. Section 5.5 presents a brief discussion of a cluster evolving in the catastrophic cooling regime when a massive black hole in the center is considered. Section 5.6 we summarize our results and conclude that below the threshold energy the stagnation radius and the accretion rate are defined by the black hole and that above the threshold line these parameters are defined by the radiative cooling. We proof also that is possible to find a smooth, stationary solution, which relates the inner subsonic accretion flow to the outer supersonic star cluster wind.

Chapter 6, as a summary, presents the main contributions of this thesis.

Chapter 2

The isothermal solution for star cluster winds

Abstract

Here we describe a simplified isothermal model of the gaseous outflows associated with the matter heated by the ionizing radiation supplied by the massive members of a star cluster. We consider two cases, with and without a gravitational field. The equations of motion are solved for two regions: within the star cluster volume, $r \leq R_{sc}$*, and that outside of* R_{sc}*. We show that there is a unique transonic solution for a particular central density value, which is found numerically. The results of numerical calculations for different star cluster parameters are presented.*

2.1 Introduction

In this chapter we describe the structure of an isothermal star cluster wind in which the injected gas is under the effects of two forces only: the inward force of gravity and the outward thermal pressure gradient. The star cluster wind model consists of a spherically symmetric star cluster with a number of massive stars which lose matter continuously. We suppose that the UV photons coming from the massive stars ionize the ejected gas and maintain the reinserted matter at a constant temperature.

We find that the hydrodynamic equations have different solutions depending on the gas central density, but there is only one solution, the so-called *critical solution* for the flow, that starts in the subsonic regime, passes through the critical radius with sonic velocity and then reaches a supersonic velocity at large distances. We use l'Hopital rule to find the asymptotic form of the equations in the vicinity of the critical radius where the equation of motion has a singularity. The critical solution occurs only for one central gas density value, which is found by an iterative method. The results of numerical calculations for both cases, with and without gravity terms, are presented in sections 2.2 and 2.3, respectively. In section 2.4 we discuss the isothermal assumption. Section 2.5 summarizes our results and conclusions.

2.2 Isothermal winds, the stationary solution

In this section we present the conservation equations of mass and momentum in spherical coordinates, and solve them for the case when the injected gas is under the effects of the star cluster gravitational field and the thermal pressure. The equation of energy conservation is simplified by the isothermal condition, which assumes that temperature is constant across the flow.

2.2.1 Main equations

The main flow equations within the star cluster volume, $r \leq R_{sc}$.

The mass conservation equation within the cluster volume is:

$$\frac{1}{r^2}\frac{d}{dr}\left(\rho u r^2\right) = q_m, \tag{2.1}$$

where, ρ and u are the gas density and the velocity of the flow, respectively, at a distance r from the center, and $q_m = 3\dot{M}_{sc}/4\pi R_{sc}^3$ is the mass deposition rate per unit volume for a constant mass deposition rate, $\dot{M}_{sc}$, of the cluster.

If the pressure gradient and gravity pull are the only forces defining the gas motion, then the momentum equation has the form:

$$u\frac{du}{dr} + \frac{1}{\rho}\frac{dP}{dr} + \frac{GM(r)}{r^2} = -\frac{q_m u}{\rho} \tag{2.2}$$

where P is the gas pressure at r and $M(r) = M_{sc}r^3/R_{sc}^3$ is the mass within the radius r, for an assumed homogeneous distribution of stars. If the injected matter cools down fast and then is photoionized by the ionizing radiation supplied by the massive members of the stellar cluster, the temperature of the gas can be approximated as a constant value. In this case the equation of energy conservation is replaced by the isothermal condition.

$$T(r) = T = constant. \tag{2.3}$$

Equation (2.3) implies that the outflowing matter is continuously heated by the ionizing radiation supplied by the cluster. Thus, in this chapter we assume that the ionizing power of the cluster is sufficient to completely photoionize the resultant outflow. However, in section 2.4 we demonstrate that in some cases this assumption may be far from reality. Here, the pressure of the gas is in direct proportion to ρ:

$$P = k\rho T/\mu \tag{2.4}$$

where k is the Boltzmann constant and μ is the mean mass per particle, $\mu = \frac{14}{23}m_H$ for a completely ionized plasma with normal cosmic abundance and m_H is the mass of the hydrogen atom.

Integrating equation (2.1), one can obtain

$$\rho = \frac{q_m r}{3u} + \frac{C}{r^2 u}. \tag{2.5}$$

The finite density at the star cluster center requires the constant of integration, C, to be zero: $C = 0$. The density of the outflow is then:

$$\rho = \frac{q_m r}{3u}. \tag{2.6}$$

Using Eq. (2.4), one can derive the pressure gradient that promotes an isothermal outflow:

$$\frac{1}{\rho}\frac{dP}{dr} = \frac{k}{\mu}\frac{dT}{dr} + \frac{kT}{\mu\rho}\frac{d\rho}{dr} = \left(\frac{kT}{\mu}\right)\frac{1}{\rho}\frac{d\rho}{dr}, \tag{2.7}$$

where the density gradient can be obtained from equation (2.6)

$$\frac{1}{\rho}\frac{d\rho}{dr} = \frac{1}{r} - \frac{1}{u}\frac{du}{dr}. \tag{2.8}$$

The substitution of equation (2.7) and (2.8) into (2.2) yields

$$u\frac{du}{dr} + \left(\frac{kT}{\mu}\right)\left[\frac{1}{r} - \frac{1}{u}\frac{du}{dr}\right] + \frac{GM(r)}{r^2} + \frac{3u^2}{r} = 0. \tag{2.9}$$

The term $3u^2/r$ in equation (2.9) makes the analytic integration difficult. This equation may also be written in a more convenient form:

$$\frac{1}{u}\frac{du}{dr} = \frac{1}{r}\frac{\left(\frac{V_{esc}^2}{2} + c_s^2 + 3u^2\right)}{(c_s^2 - u^2)} \tag{2.10}$$

where $c_s = (kT/\mu)^{1/2}$ is the isothermal sound speed, which is a constant, and $V_{esc}^2 = 2GM(r)/r$ is the square of the escape velocity at radius r. Note that inside the cluster, du/dr remains positive if the outflow is subsonic, $u < c_s$.

An analysis of equation (2.10) leads to an unexpected conclusion: the gas inside massive clusters (large V_{esc}) accelerates faster than that inside their low mass counterparts with the same radius, despite the fact that they have a larger potential well. This occurs because the gas in the subsonic region is in a quasi-hydrostatic regime and it is not dominated by the velocity law (see the analysis in Appendix A). This result is analogous to that of an isothermal wind of a single star (see Lamers & Cassinelli 1999).

The main flow equations outside the cluster, $r > R_{sc}$.

As outside the stellar cluster there is no mass deposition, then $q_m = 0$. Thus, for $r > R_{sc}$ the main hydrodynamic equations are

$$\frac{1}{r^2}\frac{d}{dr}\left(\rho u r^2\right) = 0, \tag{2.11}$$

$$u\frac{du}{dr} + \frac{1}{\rho}\frac{dP}{dr} + \frac{GM_{sc}}{r^2} = 0, \tag{2.12}$$

$$T(r) = T. \tag{2.13}$$

Following the procedure described in the previous section, one obtains:

$$\rho u r^2 = C. \tag{2.14}$$

From the stationary condition, we get that the integration constant is, $C = \dot{M}_{sc}/4\pi$. The density of the gas is then

$$\rho = \frac{\dot{M}_{sc}}{4\pi u r^2}. \tag{2.15}$$

Substituting the derivatives of density and pressure into equation (2.12) one can obtain:

$$u\frac{du}{dr} + \frac{kT}{\mu}\left[-\frac{1}{u}\frac{du}{dr} - \frac{2}{r}\right] + \frac{GM_{sc}}{r^2} = 0. \tag{2.16}$$

This equation may be rewritten in the form

$$\frac{1}{u}\frac{du}{dr} = \frac{2}{r}\frac{(c_s^2 - V_{esc}^2/4)}{(u^2 - c_s^2)}. \tag{2.17}$$

An analysis of equation (2.17) shows that it has a critical point at

$$r = r_c \equiv \frac{GM_{sc}}{2c_s^2}. \tag{2.18}$$

At this distance the numerator of equation (2.17) is equal to zero. Note that if $r < r_c$ the numerator of the equation (2.17) is negative, and thus the velocity gradient is positive if $u(r) < c_s$ and negative if $u(r) > c_s$. In the region outside the critical radius, $r > r_c$, the numerator of equation (2.17) is positive and the velocity gradient is negative if $u(r) < c_s$ and positive if $u(r) > c_s$.

2.2.2 The isothermal solution

From equation (2.17) we know that if $u(r_c) \neq c_s$, the derivative of the velocity at the critical radius is zero and the outflow remains subsonic everywhere. On the other hand, the derivative of the expansion velocity at the sonic radius, r_{sonic}, goes to infinity, unless $u(r_c) = c_s$. Thus the smooth transition from the subsonic to the supersonic regime requires that the critical point coincides with the sonic point,

$$u(r_c) = c_s = \frac{V_{esc}(r_c)}{2} \tag{2.19}$$

where $V_{esc}(r_c)$ is the escape velocity at the critical point. Thus there is only one solution which has a positive velocity gradient at all distances from the star cluster center. This is the *critical solution* which has

$$u(r_c) = c_s \quad \text{at} \quad r_c = \frac{GM_{sc}}{2c_s^2}. \tag{2.20}$$

The critical radius remains outside the cluster if

$$GM_{sc}/2c_s^2 > R_{sc} \quad \text{or} \quad V_{esc}(R_{sc}) > 2c_s. \tag{2.21}$$

In order to avoid a singularity at the critical point, and integrate equations (2.10) and (2.17) numerically, we apply l'Hopital 's rule to equation (2.17), see Appendix B, that results in

$$\frac{1}{u}\left(\frac{du}{dr}\right)_{r_c} = \left[-\frac{2c_s^2}{r_c^2} + \frac{2GM_{sc}}{r_c^3}\right]\left[\frac{2u\,du}{dr}\right]^{-1}_{rc} = \frac{c_s^2}{r_c^2}\left(\frac{u\,du}{dr}\right)^{-1}_{r_c}. \tag{2.22}$$

Which implies that a smooth transition from the subsonic to the supersonic regime requires that at $r = r_c$

$$\left(\frac{du}{dr}\right)_{r_c} = \frac{2c_s^3}{GM_{sc}}. \tag{2.23}$$

We use equation (2.23) in the vicinity of the critical point in our scheme to integrate numerically.

The results of the numerical integration for a star cluster whose parameters are: $R_{sc} = 10$ pc, $M_{sc} = 3.3 \times 10^6 M_\odot$ and ionization temperature, $T = 10^4$K, are presented

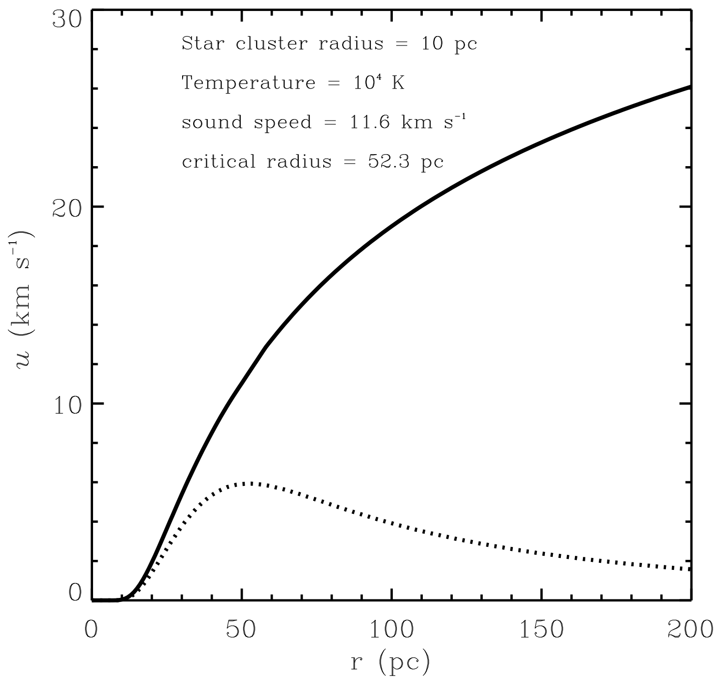

Figure 2.1: The critical and the breeze isothermal solutions, solid and dashed lines, respectively. For the critical solution the critical radius is outside the cluster volume. The breeze solution remains subsonic everywhere and has a maximum at r_c. We used a star cluster with mass $M_{sc} = 3.3 \times 10^6 M_\odot$, $R_{sc} = 10$ pc, $T = 10^4$ K.

in Figure 2.1. The solid line represents the critical solution which starts subsonic, goes through the critical point and then reaches supersonic velocities. The dotted line represents the so-called *breeze solution*. In this case the central density is too large and the pressure gradient is not sufficient for the outflow to reach the critical radius with the sound speed and thus the expansion velocity remains everywhere subsonic with a maximum at $r = r_c$. In the critical solution the critical radius is outside the cluster volume, $r_c = 52.3$ pc, and the outflow crosses this radius with a velocity $u = c_s = 11.6$ km s^{-1}.

Figure 2.2 shows the density profiles for the critical and breeze solutions, solid and dotted lines, respectively. In the case of the wind (solid line) the density decreases

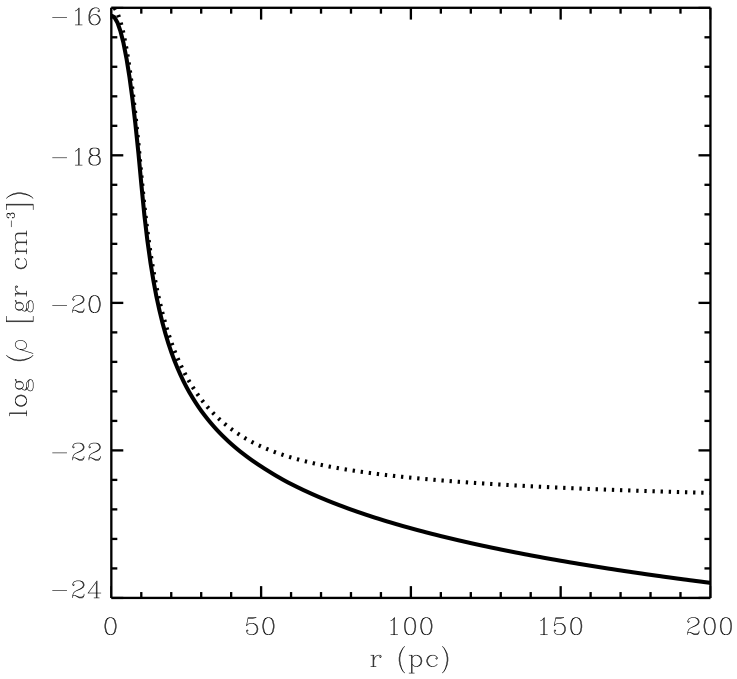

Figure 2.2: Density profiles for the critical solution (solid line) and the breeze solution (dotted line). Note that both distributions are almost equal as far as three times the cluster radius.

continuously as $\sim 1/r^2$, whereas in the breeze solution it reaches an asymptotic value at larger radii.

Analytic solution.

Note that in equation (2.10) the variables are coupled and make an analytic integration difficult. However the momentum equation (2.17) has an analytic solution which in terms of the Mach number, $\mathcal{M} \equiv u/c_s$, is

$$\frac{\mathcal{M}}{2} - \ln \mathcal{M} = \ln \xi^2 + 2\xi^{-1} - \frac{3}{2} \tag{2.24}$$

where $\xi = r/r_c$. The integration constant was fixed by the condition $u(r_c) = c_s$ at the critical radius.

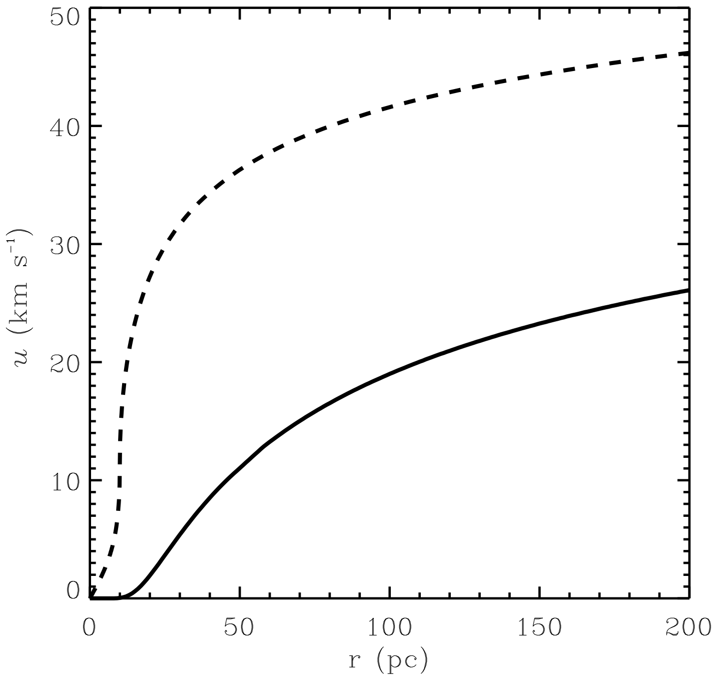

Figure 2.3: Comparison of the isothermal wind solution for the cases with and without gravity, solid line and dashed lines, respectively. When gravity term is avoided the gas accelerates faster that in the gravity case. The parameters of the cluster are $R_{sc} = 10$ pc, $M_{sc} = 3.3 \times 10^6 M_\odot$. The temperature of the gas is $T = 10^4$K.

2.3 The isothermal wind structure without gravity

If the gravity force is neglected, equations (2.10) and (2.17) take the form:

$$\frac{1}{u}\frac{du}{dr} = \frac{(c_s^2 + 3u^2)}{r\,(c_s^2 - u^2)}, \tag{2.25}$$

and

$$\frac{1}{u}\frac{du}{dr} = \frac{2c_s^2}{r\,(u^2 - c_s^2)}, \tag{2.26}$$

respectively. In this case there is no critical radius, but there is a sonic radius. The sign of equation (2.25), remains positive if $c_s > u$, while equation (2.26) is positive if $u > c_s$. Thus a smooth transition from subsonic to supersonic expansion velocities requires that the gas velocity must equal the sound speed at the star cluster surface.

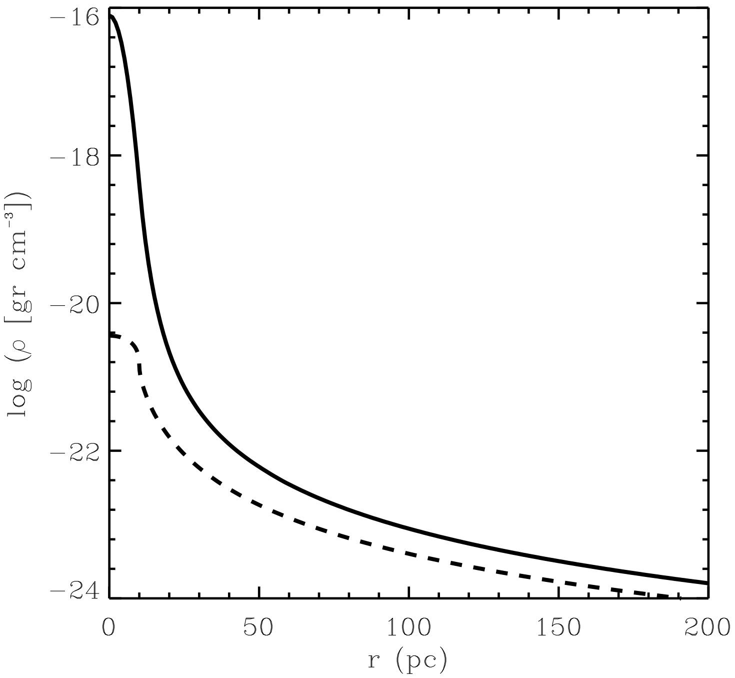

Figure 2.4: The density profiles calculated for the case with (solid line) and without (dashed line) gravity. Note that in the case with gravity term the central density is about 4 orders of magnitude larger that in the case without gravity.

The preceding analysis shows that there is a unique solution that starts subsonic and ends up as a supersonic flow. This solution occurs for a unique value of the gas central density. The results of the numerical integration of equations (2.25) and (2.26) are compared with that discussed in the previous section. Note that the gravitational field of the cluster modifies the structure of the isothermal outflow drastically. The gas in the case with gravity expands slower than in the case without it (see Figure 2.3) due to a larger central density. The central density in the case with gravity is about 4 orders of magnitude larger that in the case without it (see Figure 2.4).

Analytic solution

In general, inside the cluster the term of mass deposition $q_m = 3\rho u/r$ makes the analytic integration of equations (2.10) and (2.25) difficult. However, in the case without gravity, for $r \leq R_{sc}$, equation (2.25) has an analytic solution, which in terms of the Mach number, is

$$\mathcal{M}\left(\frac{4}{1+3\mathcal{M}}\right)^{2/3} = \xi. \tag{2.27}$$

Equation (2.27) results after applying exponentials in the integral solution.

For $r \geq R_{sc}$, equation (2.26) also has a simple analytic solution, which in terms of the Mach number results in

$$\frac{\mathcal{M}-1}{2} - \ln \mathcal{M} = \ln \xi^2, \tag{2.28}$$

where, $\xi = r/R_{sc}$. The integration constant in (2.27) and (2.28) is fixed by the condition $u(R_{sc}) = c_s$ at the cluster surface.

2.4 Problems with the isothermal assumption

The isothermal scenario assumes that the UV photons coming from the massive stars of the cluster are sufficient to keep the outflow completely ionized. But in some cases this assumption may be far from reality as shown in this section.

In a coeval starbursts, the production of UV photons remains constant until the massive stars of the cluster move away from the main sequence, to finally explode as supernovae. Before the first explosion the UV photon flux remains constant, and is given by

$$S_{UV} = S_0 \frac{M_{SB}}{M_{LH}} \tag{2.29}$$

where the initial constant flux, S_0, is normalized to the standard model of Leitherer & Heckman (1995), $S_0 = 9 \times 10^{52}$ photons s^{-1} , M_{SB} is the mass of the starbursts and $M_{LH} = 10^6 M_\odot$. For the star clusters described in the previous sections, $M_{SB} =$

$3.3 \times 10^6 M_\odot$, the photon flux is $S_{UV} \sim 10^{53}$ photons s^{-1}, then it is possible to estimate the size of the ionized region by means of the Strömgren sphere (Strömgren, 1939)

$$R_{St} = \left(\frac{S_{UV}}{\frac{4}{3}\pi \beta_2 n_H^2} \right)^{1/3} , \tag{2.30}$$

where the recombination coefficient to levels greater than the fundamental level is $\beta_2 \sim 2.6 \times 10^{-13}$ cm^3 s^{-1}, which is valid for $T = 10^4$K, and n_H is the hydrogen atom number density. For the case with gravity, we found that the central number density of hydrogen atoms is $n_H \sim 10^7$ cm^{-3}. Using this density in the equation (2.30) one obtains a Strömgren radius $R_{St} \sim 10^{17}$ cm, less than one parsec! In the case without gravity, for $r < R_{sc}$, the gas density of the outflow remains almost constant with value $n_H \sim 2 \times 10^3$ cm^{-3}, putting this into equation (2.30) one obtains a Strömgren sphere of radius $R_{St} \sim 10$ pc. This implies that outside of the cluster there are not sufficient ionizing photons to keep the outflow at a constant temperature.

The previous analysis shows that there are not sufficient ionizing photons to guarantee the isothermal condition. However, the isothermal wind model has allowed us to understand the impact of gravity in the acceleration of the gaseous outflow and its density distribution.

2.5 Conclusions

We have shown that there are many solutions for isothermal winds, depending on the initial conditions at the star cluster center. There is, however, only one critical solution for which the outflow is transonic. This solution passes through the critical radius with $u(r_c) = c_s = V_{esc}(r_c)/2$, and is known as the isothermal wind solution. This implies that in the case of a wind, the critical radius coincides with the sonic point. This condition also selects a unique central gas density.

We demonstrated that the gravitational potential of the cluster modifies drastically the structure of the isothermal gaseous outflow, leaving a large central gas density which impedes pressure gradients accelerating it efficiently.

The isothermal assumption does not represent reality very well, because the ionizing photons coming from massive stars are not sufficient to maintain the star cluster volume ionized. In both cases with and without gravity, the ionized region is smaller than the star cluster volume. However, even though the isothermal assumption is the simplest case, it has allowed us to understand how the hydrodynamics of star cluster winds are modified when gravity is considered and has also provided us with the tools to handle more sophisticated models, as described in the forthcoming chapters.

Chapter 3

The impact of gravity on radiative star cluster winds

Abstract

Super stellar clusters have masses of several thousands to a few millions of solar masses and can contain more than 10^4 *massive stars concentrated in a few parsecs. Masses of central starbursts detected around AGNs are even larger and may reach* $10^{10} M_\odot$*. Massive stars lose a significant fraction of their mass due to stellar winds and supernova explosions. Here we focus on the powerful gaseous outflows (star cluster winds) that result from the thermalization of the injected material within the volume occupied by the cluster. We have incorporated the gravity terms into the main hydrodynamic equations. The results of numerical calculations that take into account both the impact of radiative cooling and gravity, are presented.*

3.1 Introduction

A pioneering model for star cluster winds was proposed by Chevalier and Clegg (1985). This model is based on the assumption that, within a star cluster with radius R_{sc}, the matter injected by massive stars in the form of individual stellar winds and supernova ejecta is fully thermalized via random collisions promoted by the large stellar density. Thermalization implies the conversion of the stellar winds and supernova kinetic energy into thermal energy. Thus, thermalization results in a large central overpressure that continuously accelerates the injected matter from zero velocity at the center to the local sound speed at R_{sc}, allowing the gas to escape from the cluster, establishing a stationary outflow.

Chevalier and Clegg (1985), and more recently Cantó et al. (2000), presented analytic solutions to the problem. The analytic solutions have been confirmed by means of 3D adiabatic numerical calculations (see Cantó et al. 2000; Raga et al. 2001). They considered the wind as a steady state adiabatic flow coming from a spherically symmetric star cluster with a homogeneous stellar distribution and negligible gravity. However, in the case of massive and compact clusters, the temperature profile of the winds could be different from that predicted by the adiabatic model if radiative cooling is taken into account (see Silich et al. 2004).

In this chapter we take one step forward, by taking into consideration the impact of gravity due to the stellar cluster. Following the scheme proposed by Silich et al. (2004), we assume a spherically symmetric star cluster of radius R_{sc} with a large number of interacting stellar winds and supernova ejecta. The thermalization of the ejected material then results in a high central over-pressure that accelerates the ejected gas and establishes a star cluster wind. Section 3.2 shows the basics of the adiabatic case. In section 3.3 we include gravity force in the conservation equations and solve them numerically, and present results for different star cluster parameters. Section 3.4 summarizes our results.

3.2 The adiabatic solution

The main hydrodynamic equations that govern the steady state adiabatic solution are the mass, the momentum and the energy conservation equations. For the region $r \leq R_{sc}$, they are:

$$\frac{1}{r^2}\frac{d}{dr}\left(\rho_w u_w r^2\right) = q_m, \tag{3.1}$$

$$\rho_w u_w \frac{du_u}{dr} = -\frac{dP_w}{dr} - q_m u_w, \tag{3.2}$$

$$\frac{1}{r^2}\frac{d}{dr}\left[\rho_w u_w r^2 \left(\frac{u_w^2}{2} + \frac{\gamma}{\gamma - 1}\frac{P_w}{\rho_w}\right)\right] = q_e, \tag{3.3}$$

where r is the spherical radius, u_w, ρ_w and P_w are the wind velocity, density and thermal pressure, respectively (the suffix w refers to wind parameters). In Equations (3.1)-(3.3), $q_m = 3\dot{M}/4\pi R_{sc}^3$ and $q_e = 3L_{sc}/4\pi R_{sc}^3$ are the mass and energy deposition rates per unit volume, respectively.

Outside of the star cluster, $q_e = q_m = 0$, then the set of main equations for $r > R_{sc}$ is:

$$\frac{1}{r^2}\frac{d}{dr}\left(\rho_w u_w r^2\right) = 0, \tag{3.4}$$

$$\rho_w u_w \frac{du_u}{dr} = -\frac{dP_w}{dr}, \tag{3.5}$$

$$\frac{1}{r^2}\frac{d}{dr}\left[\rho_w u_w r^2 \left(\frac{u_w^2}{2} + \frac{\gamma}{\gamma - 1}\frac{P_w}{\rho_w}\right)\right] = 0. \tag{3.6}$$

The analytic solutions for the set of equations (3.1)-(3.3) and (3.4)-(3.6) are (see Cantó et al. 2000):

$$v\left[1 + \frac{(5\gamma + 1)}{(\gamma - 1)}v^2\right]^{-(3\gamma+1)/(5\gamma+1)} = Ar, \tag{3.7}$$

for the case $r \leq R_{sc}$, where they introduced the dimensionless variable $v = u_w/V_{A,\infty}$ and the constant A

$$A = \left(\frac{\gamma - 1}{\gamma + 1}\right)^{1/2} \left(\frac{\gamma + 1}{6\gamma + 2}\right)^{(3\gamma+1)/(5\gamma+1)} . \tag{3.8}$$

Outside of the cluster the solution is

$$v\left(1 - v^2\right)^{1/(\gamma-1)} = \frac{B}{r^2}, \tag{3.9}$$

where the constant B is

$$B = \left(\frac{\gamma - 1}{\gamma + 1}\right)^{1/2} \left(\frac{2}{\gamma + 1}\right)^{1/(\gamma-1)} . \tag{3.10}$$

Equations (3.7) and (3.9) together with constants A and B completely define the analytic solution. For the central region, i.e., for small values of r, the expansion velocity grows almost linearly, whereas the temperature and density remain almost homogeneous. However, outside of the star cluster, the hydrodynamic variables rapidly approach their asymptotic values: $u_w \rightarrow V_{A,\infty}$, $\rho_w \sim r^{-2}$, $T \sim r^{-4/3}$ and $P \sim r^{-10/3}$.

Physically, there are three star cluster parameters that together define the hydrodynamic properties of the adiabatic wind outflow, or the distribution of density $\rho_w(r)$, temperature $T_w(r)$ and expansion velocity $u_w(r)$ as functions of distance from the cluster center: they are the mean mechanical luminosity, L_{sc}, the mass deposition rate, $\dot{M}_{sc}$, and the size of the stellar cluster, R_{sc}. The total mass and energy deposition rates also define the adiabatic wind terminal velocity, $V_{A,\infty}$:

$$V_{A,\infty} = \left(\frac{2L_{sc}}{\dot{M}}\right)^{1/2} \tag{3.11}$$

The central parameters in the adiabatic case are (see Cantó et al. 2000):

$$\rho_c = \frac{\dot{M}_w}{4\pi A R_{sc}^2 V_{A,\infty}}, \tag{3.12}$$

$$P_c = \frac{\gamma - 1}{2\gamma} \frac{\dot{M}_w V_{A,\infty}}{4\pi A R_{sc}^2}, \tag{3.13}$$

$$c_c = \sqrt{\frac{\gamma - 1}{2}} V_{A,\infty}, \tag{3.14}$$

$$T_c = \frac{\gamma - 1}{\gamma} \frac{\mu}{k} \frac{q_e}{q_m}. \tag{3.15}$$

Using these initial values one can solve the conservation equations (Eqs. 3.1-3.3 and 3.4-3.6) numerically and reproduce the analytic wind solution.

3.3 The radiative solution with gravity

More realistic models of star cluster winds must include radiative cooling and gravity. The effects of radiative cooling have been discussed in Silich et al. (2004). In this section we discus the impact of gravity on the hydrodynamics and the structure of radiative star cluster winds.

3.3.1 Main equations

The set of equations that includes the gravitational pull of the cluster are similar to those in Holzer and Axford (1970), but here we also include radiative cooling. For $r \le R_{sc}$ they are:

$$\frac{1}{r^2} \frac{d}{dr} \left(\rho_w u_w r^2 \right) = q_m, \tag{3.16}$$

$$\rho_w u_w \frac{du_w}{dr} = -\frac{dP_w}{dr} - q_m u_w - \frac{G \rho_w M(r)}{r^2}, \tag{3.17}$$

$$\frac{1}{r^2} \frac{d}{dr} \left[\rho_w u_w r^2 \left(\frac{u_w^2}{2} + \frac{\gamma}{\gamma - 1} \frac{P_w}{\rho_w} \right) \right] = q_e - Q - \frac{G \rho_w u_w M(r)}{r^2}, \tag{3.18}$$

where $M(r)$ is the mass of the cluster as a function of the spherical radius, r. In the case of a homogeneous stellar mass distribution $M(r) = M_{sc}(r/R_{sc})^3$.

The main equations for $r \ge R_{sc}$ are:

$$\frac{1}{r^2} \frac{d}{dr} \left(\rho_w u_w r^2 \right) = 0, \tag{3.19}$$

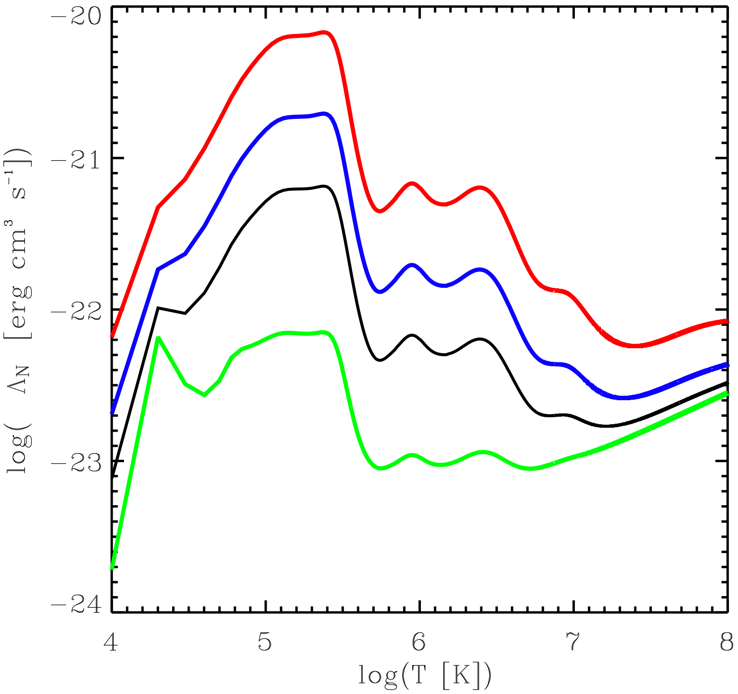

Figure 3.1: The cooling rate as a function of temperature for different metallicities of the emitting plasma. $Z = 0.1Z\odot$ (green), $Z = Z\odot$ (black), $Z = 3Z\odot$ (blue) and $Z = 10Z\odot$. (Raymond et al. 1977).

$$\rho_w u_w \frac{du_u}{dr} = -\frac{dP_w}{dr} - \frac{G\rho_w M_{sc}}{r^2}, \tag{3.20}$$

$$\frac{1}{r^2}\frac{d}{dr}\left[\rho_w u_w r^2 \left(\frac{u_w^2}{2} + \frac{\gamma}{\gamma-1}\frac{P_w}{\rho_w}\right)\right] = -Q - \frac{G\rho_w u_w M_{sc}}{r^2}. \tag{3.21}$$

The cooling rate, Q, in equations (3.18) and (3.21) is:

$$Q = n_i n_e \Lambda(Z, T), \tag{3.22}$$

where n_i and n_e are the ion and electron number densities, respectively, and $\Lambda(Z, T)$ is the cooling function, which depends on the gas temperature and metallicity, Z (see Figure 3.1). The main cooling processes are dependent on the plasma temperature: for $T \leq 10^7$ cooling is mainly due to ion de-excitation and recombination lines, and for $T > 10^7$, electron bremsstrahlung is the dominant agent (see Raymond et al. 1976; Sutherland & Dopita, 1993).

The highly nonlinear character of the cooling function makes it impossible to find the analytic solution of the hydrodynamic equations. On top of that, when cooling is added, the initial conditions become unknown. Thus, to take into account the impact of radiative cooling on the internal structure of the star cluster winds, one has to know three parameters: n_c, T_c and Z, the central density, the central temperature and the metallicity, respectively. The way to solve the problem was suggested in Silich et al. (2004). Hereafter, we follow their scheme, which enables us to solve the set of equations (3.16)-(3.21) numerically. As first step, we rewrite the conservation equations in a more convenient form.

The set of flow equations inside the star cluster, $r \leq R_{sc}$.

The integration of equation (3.16) yields:

$$\rho_w = \frac{q_m r}{3u_w} + \frac{C}{u_w r^2}, \tag{3.23}$$

where the constant of integration, C, is defined by the boundary conditions. It is equal to zero if the central density is finite. Then the density of the plasma inside the cluster is

$$\rho_w = \frac{q_m r}{3u_w}. \tag{3.24}$$

Substituting equation (3.24) into the momentum equation (3.17) we get:

$$\left(\frac{q_m r}{3}\right)\frac{du_w}{dr} = -\frac{dP_w}{dr} - q_m u_w - \frac{G\rho_w M(r)}{r^2}. \tag{3.25}$$

Note that, $M(r) = M_{sc}\left(r/R_{sc}\right)^3$, is the mass within the volume of radius r. Rearranging equation (3.25), one can obtain:

$$\frac{dP_w}{dr} = -q_m\left(\frac{r}{3}\frac{du_w}{dr} + u_w\right) - \frac{G\rho_w M(r)}{r^2}. \tag{3.26}$$

On the other hand, substituting equation (3.24) into equation (3.18) we obtain

$$\frac{1}{r^2}\frac{d}{dr}\left[\left(\frac{q_m r}{3}\right) r^2 \left(\frac{u_w^2}{2} + \frac{\gamma}{\gamma-1}\frac{P_w}{\rho_w}\right)\right] = q_e - Q - \frac{G\rho_w u_w M(r)}{r^2}. \tag{3.27}$$

Taking derivatives in the left-hand side of equation (3.27) and substituting equation (3.26), we obtain

$$\frac{du_w}{dr} = \frac{(q_e - Q)(\gamma-1) + (\gamma+1)\left(q_m u_w^2/2\right) - 2\gamma P_w u_w/r + \rho_w u_w GM(r)/r^2}{\rho_w\left(\gamma P_w/\rho_w - u_w^2\right)}. \tag{3.28}$$

The gas pressure is $P_w = c_s^2 q_m r/3\gamma u_w$. Substituting P_w into Eq. (3.28), yields

$$\frac{du_w}{dr} = \frac{(\gamma-1)(q_e - Q) + q_m\left[\frac{(\gamma+1)}{2}u_w^2 - \frac{2}{3}\left(c_s^2 - \frac{V_{esc}^2}{4}\right)\right]}{\rho_w\left(c_s^2 - u_w^2\right)}, \tag{3.29}$$

where $V_{esc}^2 = 2GM(r)/r$ is the square of the escape velocity at radius r.

Equation (3.29) together with equations (3.26) and (3.24) form the set of the main equations that define the structure of the steady state outflow inside the cluster.

The set of flow equations outside the star cluster, $r > R_{sc}$.

The integration of the mass conservation equation outside of the cluster results in

$$\rho_w = \frac{\dot{M}_{sc}}{4\pi r^2 u_w}. \tag{3.30}$$

Substitution of the Eq. (3.30) into Eq. (3.20) gives

$$\frac{dP_w}{dr} = -\frac{\dot{M}_{sc}}{4\pi r^2}\frac{du_w}{dr} - \frac{\rho_w GM_{sc}}{r^2}. \tag{3.31}$$

The energy conservation, Eq. (3.21), may be rewritten in the form

$$\frac{d}{dr}\left[\rho_w u_w r^2\left(\frac{u_w^2}{2} + \frac{\gamma}{\gamma-1}\frac{P_w}{\rho_w}\right)\right] = -Qr^2 - \rho_w u_w GM_{sc}. \tag{3.32}$$

Combining Eq. (3.30) and Eq. (3.31) then results in

$$\left(\gamma P_w - \rho_w u_w^2\right)\frac{du_w}{dr} = \left(-Q - \frac{\rho_w u_w GM_{sc}}{r^2}\right)(\gamma-1) - \frac{2\gamma P_w u_w}{r} + \frac{\gamma\rho_w u_w GM_{sc}}{r^2} \tag{3.33}$$

Finally, replacing the thermal pressure by the sound speed, c_s, as it was done in the previous section,

$$\frac{du_w}{dr} = \frac{1}{\rho_w} \frac{(\gamma - 1) r^2 Q + 2 r u_w \rho_w \left(c_s^2 - V_{esc}^2/4\right)}{r^2 \left(u_w^2 - c_s^2\right)}. \tag{3.34}$$

Equations (3.30), (3.31) and (3.34) form the set of the main equations outside of the star cluster volume.

3.3.2 Numerical results and discussion.

If, at the star cluster surface, the sound speed exceeds one half of the escape velocity, the steady state outflow is possible. The smooth transition from the subsonic to the supersonic solution then requires that the velocity of the plasma equals the sound speed at the star cluster surface. The derivative of the expansion velocity then remains positive throughout the space (see Silich et al. 2004).

There are three possible types of the integral curves that result from different positions of the sonic point (see Silich et al. 2004):

1. R_{sonic} coincides with the radius of the star cluster, R_{sc}. In this case the stationary wind solution is possible. The thermal presure decreases continuously inside and outside the star cluster and approaches a negligible value at large radii. The expansion velocity grows from zero km s^{-1} at the center, to the local sound speed at the star cluster surface and then reaches its terminal value, $V_{A,\infty}$, which is ~ 2 times the sound speed at the star cluster surface.

2. The sonic point is outside the star cluster, $R_{sonic} > R_{sc}$. In this case the breeze solution sets in. The central density is larger than that in the wind solution. The pressure gradient inside the cluster is not sufficient for the ejected material to reach the supersonic velocity and the outflow remains subsonic everywhere. The expansion velocity decreases abruptly and goes to zero km s^{-1} outside of the star cluster surface.

3. The expansion velocity reaches the sonic value inside the cluster, $R_{sonic} \leq R_{sc}$. In this case the formal solution is double-valued which implies that it has no physical meaning.

Thus, in order to find the stationary wind solution, we have to choose the appropriate central parameters (ρ_c and T_c) that accommodate the sonic point at the star cluster surface. This is the key point that allows the numerical integration of the hydrodynamic equations (3.26)-(3.29) and (3.31)-(3.34). To find the central conditions, we compare Eq. (3.29) at $r = 0$, where $u_w = 0$, with the derivative of the velocity from the equation (3.24) evaluated at $r = 0$:

$$\frac{q_m}{3}\frac{1}{\rho_c} = \frac{1}{\rho_c}\frac{(\gamma - 1)\left[q_e - n_c^2 \Lambda(Z, T_c)\right] - \frac{2}{3} q_m c_c^2}{c_c^2} \tag{3.35}$$

Equation (3.35) defines the relation between the density and the temperature of the plasma at the star cluster center:

$$n_c = \left[\frac{q_e - q_m c_c^2/(\gamma - 1)}{\Lambda(Z, T_c)}\right]^{1/2} = q_m^{1/2}\left[\frac{V_{A,\infty}^2/2 - c_c^2/(\gamma - 1)}{\Lambda(Z, T_c)}\right]^{1/2}, \tag{3.36}$$

where $V_{A,\infty}^2 = 2q_e/q_m$. In the absence of radiative cooling one can recover from equation (3.36) the value of the adiabatic temperature at the center (see equation 3.15). Note, that equation (3.36) may be also derived from the equation of energy conservation (see, for example, Sarazin & White III 1987).

Thus to perform the numerical integration, one has to iterate the central temperature until the sonic point reaches the star cluster surface. The central temperature has a maximum which corresponds to the adiabatic value, $T_{max} = [\gamma - 1/\gamma](\mu/k)(q_e/q_m)$. When the central temperature approaches the adiabatic value, the sonic point goes to zero (see Figure 3.2) and, consequently, the central density and pressure also go to zero (see eq. 3.36). For smaller values of T_c, the sonic radius and the central pressure grows until they reach a maximum at some critical temperature (T_{crit}), the maximum in pressure is bounded by the gas radiative cooling (Silich et al. 2004). If the central temperature becomes even smaller that T_{crit}, there is a fall in pressure promoted by

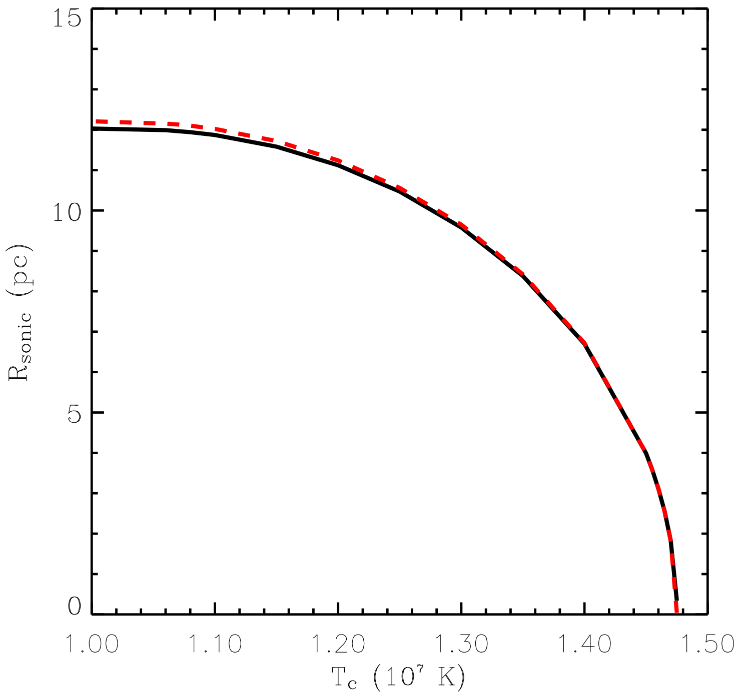

Figure 3.2: Position of the sonic point for a star cluster with $R_{sc} = 7$ pc and $V_{A,\infty} = 1000\,\mathrm{km\,s^{-1}}$. The outflow has solar metallicity. The solid line results from the model with gravity. Dotted line is the case without gravity. In this particular case the adiabatic temperature is $T_{max} \sim 1.47 \times 10^7$ K and the critical temperature $T_{crit} = 10^7$ K.

radiative cooling, this effect is called catastrophic cooling. In such conditions the central pressure cannot promote an effective outward accreleration. Therefore, in the radiative case the sonic radius (R_{sonic}) cannot be arbitrarily large and has a maximum value for any given set of star cluster parameters. The parameters of the cluster for which the sonic radius and pressure take their maximum value define the critical luminosity of the cluster.

One can find the critical luminosity for any set of star cluster parameters if one fixes T_{crit} that corresponds to the maximum sonic radius and then iterates the star cluster mechanical luminosity until the sonic point reaches the star cluster surface. This critical luminosity is plotted in Figure 3.3 (black line), and is compared with

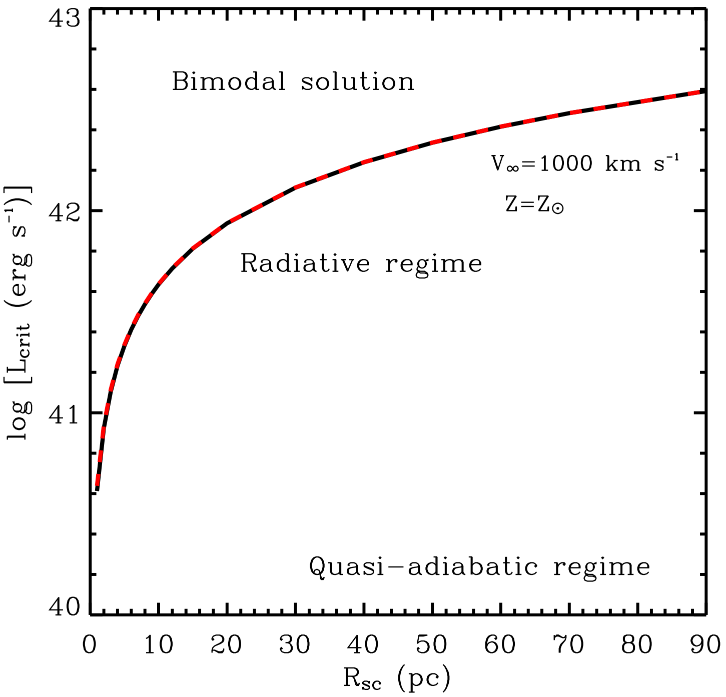

Figure 3.3: The threshold energy input rate as a function of the star cluster radius. Above the line, the bimodal solution with the stagnation radius $0 < R_{st} < R_{sc}$ sets in. Star clusters whose mechanical luminosity is close to the critical value blow away material in the strongly radiative regime. Far below the line, the wind is quasi-adiabatic. The figure shows models with (solid line) and without (red dashed line) gravity. For larger values of the terminal speed the threshold line moves upward.

that from Silich et al. (2004) (red dashed line) for star cluster winds with solar metallicity, $Z_{\odot}$, and adiabatic terminal velocity, $V_{A,\infty} = 1000\,\mathrm{km\,s^{-1}}$. One can see that gravity pull from the cluster does not change the location of the threshold line. This is because the gravitational energy is smaller than the thermal energy at any distance from the star cluster center. One can see this by comparing the escape velocity, $V_e \simeq 100\,\mathrm{km\,s^{-1}}$ with the local sound speed, $c_s \sim 400\,\mathrm{km\,s^{-1}}$, at the star cluster surface.

In Figure 3.3 if the luminosity of the star cluster is smaller than the critical value,

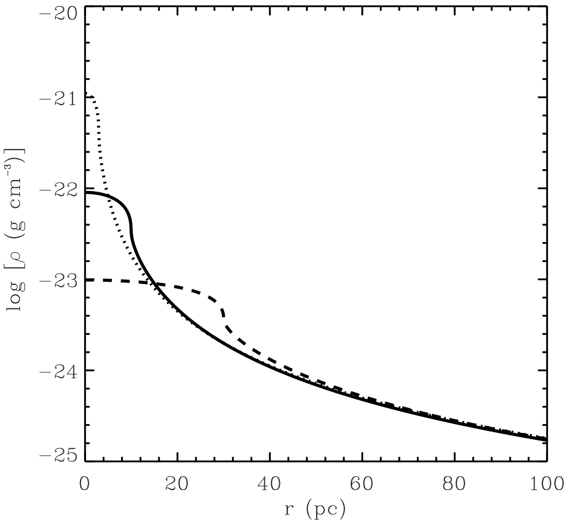

Figure 3.4: Star cluster wind density distributions for three star cluster models: $R_{sc} = 3$ pc (dotted line), $R_{sc} = 10$ pc (solid line) and $R_{sc} = 30$ pc (dashed line). All of these with mass $M_{sc} = 10^6 M_\odot$, mechanical luminosity $L_{sc} = 10^{41}\,\mathrm{erg\,s^{-1}}$ and adiabatic wind terminal velocity $V_{A,\infty} = 1000\,\mathrm{km\,s^{-1}}$. Note that the most compact cluster has the larger central density and thus in this case the radiative cooling becomes very important.

the star cluster wind is in a quasi-adiabatic regime. If the luminosity approaches the critical value, the wind becomes strongly radiative. When the luminosity exceeds the critical value, catastrophic cooling sets in the central region (see Silich et al. 2004) and the stagnation point (the point where $u_w = 0$) moves away from the center and the cluster evolves into a bimodal regime in which the central, densest zones cool rapidly and accumulate the injected matter, while the outer zones are still able to drive a stationary wind (see Tenorio-Tagle et al. 2007).

The results of the numerical calculations that include the gravitational pull of clusters with mass, $M_{sc} = 10^6 M_\odot$, mechanical luminosity, $L_{sc} = 10^{41}\,\mathrm{erg\,s^{-1}}$, and radii, $R_{sc} = 3$pc (dotted line), 10pc (solid line) and 30 pc (dashed line), respectively, are presented in Figures 3.4a, 3.4b and 3.4c. The most compact star cluster presents the largest central densities, two orders of magnitude larger if compared to the $R_{sc} =$

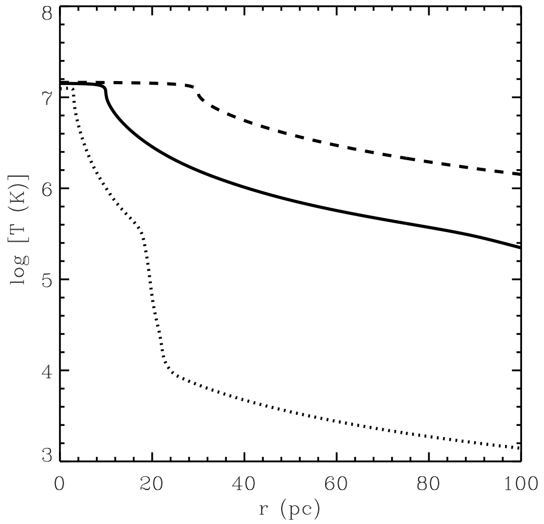

Figure 3.4b.—Temperature distributions for the clusters described in Figure 3.4a. The most compact cluster (dotted line) strongly departs from the adiabatic solution as a result of radiative cooling. Note that for larger R_{sc} the solution approaches the adiabatic case (solid and dashed lines).

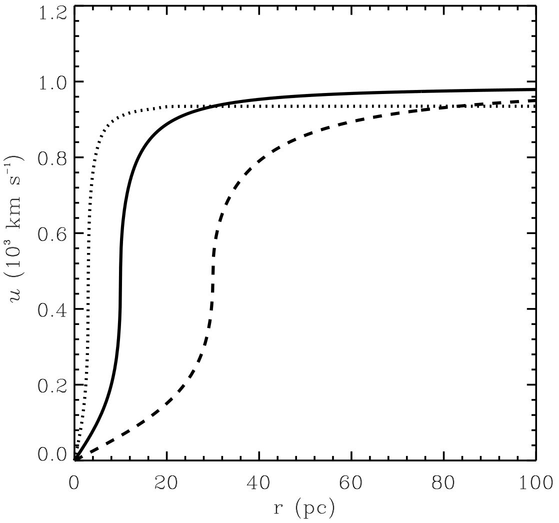

Figure 3.4c.— Wind velocity profiles for the three clusters described in the text. More compact clusters (dotted line) accelerates the gas more efficiently than larger ones (solid and dashed lines).

30 pc case (see Figure 3.4a). Note that inside the clusters, temperature remains almost constant (see Figure 3.4b). In the most compact cluster the temperature drops down quickly, about two orders of magnitude within the first 20 pc, while in the largest cluster the temperature profile follows a quasi-adiabatic solution. Figure 3.4c shows that the outflow in the most compact cluster accelerates faster than in clusters with the same mass but larger radii. In all these calculations gravity does not significantly change the radiative model of Silich et al. (2004).

3.4 Conclusions.

In this chapter we have incorporated the gravity terms into the main hydrodynamic equations and presented the results of numerical calculations that take into consideration both, the impact of radiative cooling and gravity. We found that the gravitational pull from the star cluster does not modify significantly the radiative solution found by Silich et al. (2004).

We demonstrate that in more compact clusters, the gas accelerates more rapidly despite the larger gravitational pull. This is because the pressure gradient is larger in the case of compact clusters.

In the next chapters we will consider the impact of a supermassive black hole placed at the center of the star cluster as it has been inferred in the case of composite AGN-SB galaxies, in bulges of non-active galaxies and in massive clusters.

Chapter 4

Steady-state spherically symmetric accretion

Abstract

The high luminosities associated with AGNs require an effective energy production mechanism. One of the most efficient mechanisms known in astrophysics is the accretion of matter onto a massive compact object. It may convert the rest mass energy of the accreted material into radiation with an efficiency up to $\sim$ *10%.*

In this chapter we present and solve numerically the main equations for spherically symmetric accretion onto the massive central object. We analyze how the mass accretion rate changes with the mass of the central black hole and apply our results to the nuclear region of the galaxy M87. We derive the position of the sonic point and the radius (the accretion radius) at which gravity becomes an important factor. The mass accretion rate and the expected luminosity for M87 are also calculated and compared with observations.

4.1 Introduction

In the accretion problem if all the kinetic energy of in-falling matter onto a compact object of mass M is given up to radiation at its surface, R, the accretion luminosity is given by

$$L_{acc} = GM\dot{M}/R. \tag{4.1}$$

The efficiency of accretion as energy release mechanism is strongly dependent on the rate $\dot{M}$ at which matter is accreted. But, for a fixed value of $\dot{M}$, the luminosity of an accreting system depends on the compactness, M/R, of the accreting object. For the case of an accretion onto a black hole the accretion efficiency is less certain. Since the radius does not refer to a hard surface but only to a region into which matter can fall and from which it cannot escape, much of the accretion energy could disappear into the hole and simply add to its mass, rather than be radiated. The uncertainty in this case is parametrized by a dimension less quantity η in equation (4.1) and using $R = R_{Schw} = 2GM/c^2$, the Schwarzschild radius:

$$L_{acc} = \eta\dot{M}c^2. \tag{4.2}$$

A reasonable assumption in this case is $\eta \sim 0.1$ (see Frank et al., 2002). Hereafter we use this value for η.

The problem of gas accretion onto the central compact object was first considered in the classical study by Bondi and Hoyle (1944), and later by Bondi (1952), who found that in this case the mass accretion rate can be expressed in terms of the ambient conditions around the accreting object. In this chapter we follow this prescription. It is assumed that the compact object is spherically symmetric and at rest inside an infinite homogeneous gas cloud. Here the central issue is to know the mass accretion rate to solve the set of hydrodynamic equations. In section 4.2 we present and analyze qualitatively the main hydrodynamic equations. In section 4.3 we formally present the accretion solution by numerically solving the resulting algebraic equation. The numerical solution for different black hole masses is presented. In particular, in section 4.4 we apply the theory to the super massive BH at the center of M87. Section 4.5 presents our conclusions.

4.2 Main equations

Again, like in the previous chapters, we consider the mass, momentum and the energy conservation equations to find the steady accretion flow. For a steady state, spherically symmetric flows, the continuity equation is

$$\frac{1}{r^2}\frac{d}{dr}\left(\rho u r^2\right) = 0, \tag{4.3}$$

where ρ is the ISM gas density and u is the gas velocity at some radius r. The velocity, u, is assumed to be negative since the flow is directed inward.

In this case, the only contribution to the external force is from gravity, therefore the Euler equation takes the form:

$$u\frac{du}{dr} + \frac{1}{\rho}\frac{dP}{dr} + \frac{GM_{BH}}{r^2} = 0, \tag{4.4}$$

where P is the gas pressure, M_{BH} is the mass of the accreting object (black hole) and G is the gravitational constant. The energy conservation equation has a more complex structure and in the simplest case can be replaced by the polytropic relation

$$P = K\rho^{\gamma}, \tag{4.5}$$

where γ is the polytropic index and K is a constant.

One can derive some conditions for the gas inflow before the integration. The gradient of the pressure can be expressed as

$$\frac{dP}{dr} = \frac{dP}{d\rho}\frac{d\rho}{dr} = c_s^2\frac{d\rho}{dr}. \tag{4.6}$$

where c_s is the sound speed at a distance r from the accreting object. Hence, the term $(1/\rho)(dP/dr)$ in the momentum equation (4.4) is $(c_s^2/\rho)(d\rho/dr)$. From the continuity equation (4.3) one can obtain

$$\frac{1}{\rho}\frac{d\rho}{dr} = -\frac{1}{ur^2}\frac{d}{dr}(ur^2) \tag{4.7}$$

Therefore, equation (4.4) can be re-written in the form:

$$u\frac{du}{dr} - \frac{c_s^2}{ur^2}\frac{d}{dr}(ur^2) + \frac{GM_{BH}}{r^2} = 0. \tag{4.8}$$

And after some algebra it may be presented in the form:

$$\frac{1}{2}\left(1 - \frac{c_s^2}{u^2}\right)\frac{d}{dr}(u^2) = \frac{1}{r}\left(2c_s^2 - \frac{GM_{BH}}{r}\right). \tag{4.9}$$

The term in parentheses in the right hand side of this equation vanishes at $r = r_B$, where

$$r_B = \frac{GM_{BH}}{2c_s^2(r_B)}. \tag{4.10}$$

This is known as the *Bondi radius*. Note that at $r = r_B$ the escape velocity is two times larger than the local sound speed.

Far away from the gravitational center the flow must be subsonic because it is assumed that the gas is at rest, but the temperature and thus the speed of sound, are non-zero:

$$u^2 < c_s^2 \quad \text{for}\, r \gg r_B. \tag{4.11}$$

Note that, as the gas approaches the accreting object, the factor $(2c_s^2 - GM/r)$ in the right-hand side of equation (4.9) steadily decreases until it vanishes at the Bondi radius. For $r < r_B$, $(2c_s^2 - GM/r)$ becomes negative and to maintain the accretion regime $(du^2/dr < 0)$, $1 - c_s^2/u^2$ must be positive. This implies that for $r < r_B$, the velocity of the flow must be supersonic:

$$u^2 > c_s^2 \quad \text{for}\, r < r_B. \tag{4.12}$$

Thus, we are looking for a solution in which the flow starts with zero velocity at large radii, then its velocity becomes negative and remains subsonic until it reaches the local sound speed at $r = r_B$, to then move with supersonic velocities towards the surface of the accreting body.

A similar analysis of the signs in equation (4.9) shows that it is possible to have a *transonic* solution with subsonic velocities at small radii and supersonic velocities at large radii. This is known as a wind solution (Chapter 2, see also Holzer & Axford, 1970 and Frank et al. 2002).

4.3 The inner structure of the accretion flow

Equation (4.3) can be easily integrated:

$$r^2 \rho u = C, \tag{4.13}$$

where C is the integration constant. Since ρu is the inward flux of mass, the constant C is related to the accretion rate, $\dot{M}$, and equation (4.13) may be re-written as

$$r^2 \rho u = \frac{\dot{M}}{4\pi}. \tag{4.14}$$

Notice that so far we do not know the exact value of the accretion rate, $\dot{M}$.

One can also integrate equation (4.4), that results in:

$$\frac{u^2}{2} + \frac{K\gamma}{\gamma - 1}\rho^{\gamma-1} - \frac{GM_{BH}}{r} = C_2 \tag{4.15}$$

where C_2 is the integration constant. We have used $dP = K\gamma\rho^{\gamma} d\rho$, from the polytropic relation. The integration constant C_2 can be found from the outer boundary condition, namely, that the velocity of the gas goes to zero when $r \longrightarrow \infty$:

$$C_2 = \frac{K\gamma}{\gamma - 1}\rho_{ISM}^{\gamma-1}, \tag{4.16}$$

where ρ_{ISM} is the ISM gas density far away from the accreting body. Substituting (4.16) into (4.15) and using $K\gamma\rho_{ISM}^{\gamma-1} = c_{ISM}^2$, and $K\gamma\rho^{\gamma-1} = c_s^2$, one can obtain

$$\frac{u^2}{2} + \frac{c_s^2}{\gamma - 1} - \frac{GM_{BH}}{r} = \frac{c_{ISM}^2}{\gamma - 1}, \tag{4.17}$$

where c_{ISM} is the sound speed of the interstellar gas far away from the accreting object.

Through equation (4.17) one can relate the sound speed at the Bondi radius, c_B, with that far away from the accreting object. Indeed, using equation (4.10) and taking into account that at the Bondi radius $u^2(r_B) = c_s^2(r_B) \equiv c_B^2$, one obtains:

$$c_B = c_{ISM} \left(\frac{2}{5 - 3\gamma} \right)^{1/2}, \tag{4.18}$$

where $c_B^2 = GM_{BH}/2r_B$. The density at the sonic point can be related to the density of the ISM, ρ_{ISM}, by the polytropic relation:

$$\rho_B = \rho_{ISM} \left(\frac{c_B}{c_{ISM}} \right)^{2/\gamma - 1}. \tag{4.19}$$

This allows one to derive the accretion rate, $\dot{M}$, for stationary, spherically symmetric accretion. Indeed, at the Bondi radius

$$\dot{M} = 4\pi \rho_B c_B r_B^2. \tag{4.20}$$

Substituting equations (4.18), (4.19) and the sonic radius $r_B = GM_{BH}/2c_B^2$ into equation (4.20) one can obtain

$$\dot{M}_B = \pi G^2 M_{BH}^2 \frac{\rho_{ISM}}{c_{ISM}^3} \left(\frac{2}{5 - 3\gamma} \right)^{\frac{5-3\gamma}{2(\gamma-1)}}, \tag{4.21}$$

where $\dot{M}_B$ is known as the Bondi accretion rate. Note that it depends only on the gas parameters far away from the accreting body and on the mass of the compact object. In the stationary case $\dot{M}_B$ does not depend on the distance from the center. Observe that $\dot{M}_B$ is not defined for polytropic indexes $\gamma = 5/3$ and $\gamma = 1$. However, see Appendix C to see how to avoid these problems.

In order to find the stationary solution, equation (4.17) can be rewritten in a more convenient form

$$\frac{v^2}{2} + \frac{c_{ISM}^2}{\gamma - 1} \left[\left(\frac{\rho}{\rho_{ISM}} \right)^{\gamma - 1} - 1 \right] - \frac{GM_{BH}}{r} = 0 \tag{4.22}$$

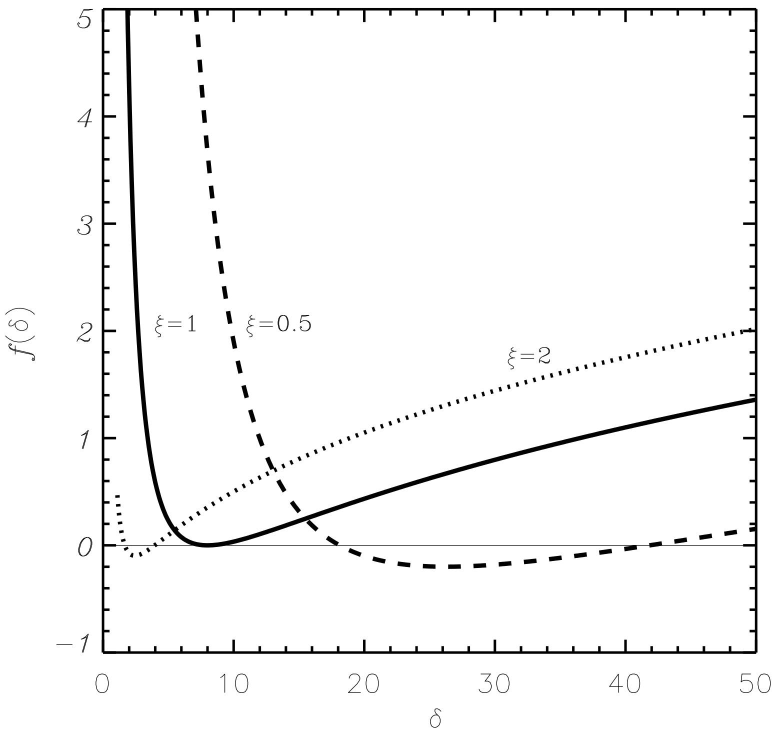

Figure 4.1: The shape of function $f(\delta,\xi)$ for different dimensionless radii, ξ. For $r = r_B$ (solid line) there is a single root. For $\xi \neq 1$ the function $f(\delta,\xi)$ has two roots, these are described in the text.

In which, if one substitutes u from equation (4.14) and, using (4.19), (4.21) and (4.10), one finds the algebraic equation that defines the distribution of density in the accretion flow:

$$\left(\frac{\rho}{\rho_{ISM}}\right)^{\gamma-1} + \frac{\gamma-1}{2}\left(\frac{r_B}{r}\right)^4 \left(\frac{\rho_{ISM}}{\rho}\right)^2 \left(\frac{2}{5-3\gamma}\right)^{\gamma+1/\gamma-1} - 4\left(\frac{\gamma-1}{5-3\gamma}\right)\frac{r_B}{r} = 1. \qquad (4.23)$$

One can rewrite this equation for the dimensionless variables, $\delta = \rho/\rho_{ISM}$ and $\xi = r/r_B$:

$$f(\delta,\xi) = \delta^{\gamma-1} + \frac{\gamma-1}{2}\xi^{-4}\delta^{-2}\left(\frac{2}{5-3\gamma}\right)^{\frac{\gamma+1}{\gamma-1}} - 4\left(\frac{\gamma-1}{5-3\gamma}\right)\xi^{-1} - 1 = 0 \qquad (4.24)$$

Figure 4.1 shows the function $f(\delta,\xi)$ for three different radii: $r = r_B$, $r = 2r_B$

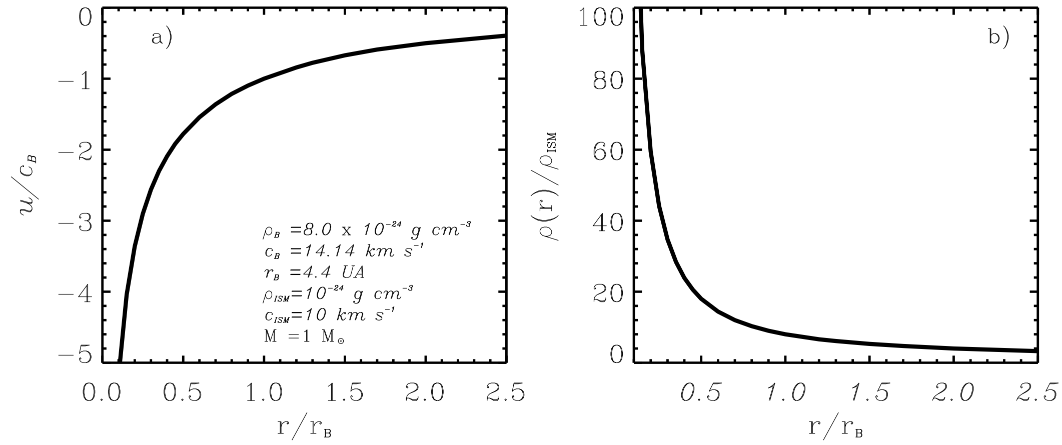

Figure 4.2: The inner structure of the accretion flow. Panel a displays the velocity profile (normalized to the sound speed at r_B) and panel b shows the density distribution (normalized to the ISM density) for the stationary, spherically symmetric accretion. The distance is also normalized to the Bondi radius. We have used a $1M_{\odot}$ object, embedded into a ISM whose particle number density is 1 cm^{-3}, temperature $T_{ISM} = 5500$ K and polytropic index $\gamma = 4/3$.

and $r = r_B/2$. For each value of ξ, the function $f(\delta, \xi)$ has two roots (see dotted and dashed lines). Only for $r = r_B$ does it have a single solution. For $\xi < 1$ (dashed line) the left-hand side root corresponds to the accretion solution and the right hand side root to the wind solution. If $\xi > 1$ (dotted line), the left hand side root corresponds to the wind solution and the right hand side root represents the accretion solution.

To construct the density distribution, $\rho(r)$, in the accretion flow we solve equation (4.24) by an iterative method for each value of ξ. Then we use equation (4.22) to find $u(r)$. Figure 4.2 presents the velocity and density profiles for an accretion flow onto a compact object with a solar mass, embedded into a gas cloud with polytropic index, $\gamma = 4/3$, particle number density, $n = 1$ cm^{-3}, and sound speed, $c_s = 10$ km s^{-1}, at large distances from the accreting body. The velocity of the flow grows as it

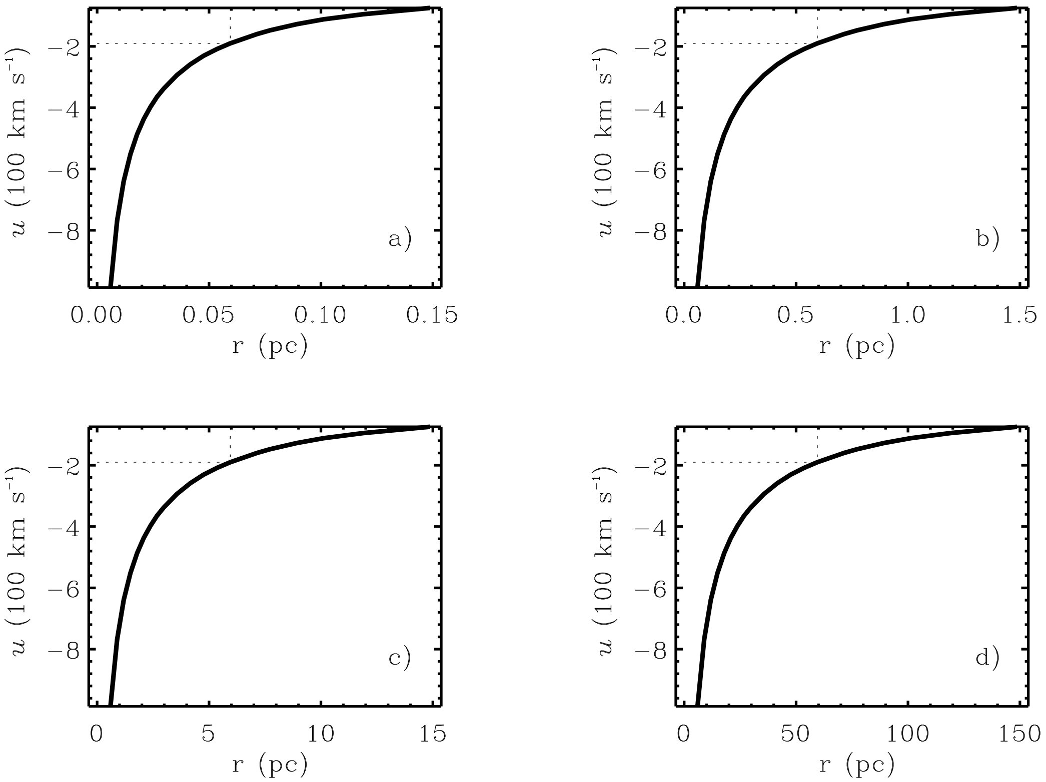

Figure 4.3: Velocity profiles for different black hole masses. Panels a, b, c and d) present results for $M_{BH} = 10^6 M_\odot$, $10^7 M_\odot$, $10^8 M_\odot$ and for $10^9 M_\odot$, respectively. The intersection of dotted lines represents the Bondi radius, r_B, it scales linearly with the mass of the BH.

approaches the accreting object, the gas moves with subsonic velocities outside of the Bondi radius, passes r_B with sonic speed ($u = c_B$) and then moves to the center with supersonic speed (see Panel a). Note that the calculated velocity is consistent with $c_B = \sqrt{2} c_{ISM}$ derived from equation (4.18). The density in the accretion flow (panel b) at $r = r_B$ is consistent with $\rho_B = 8\rho_{ISM}$ derived from equation (4.19).

For this particular case, the accretion rate is $\dot{M} = 6.26 \times 10^{11}$ g s^{-1}. Then if one assumes that the accretion efficiency is $\eta = 0.1$, one can estimate the luminosity of the accreting object, in this case:

$$L_{acc} = \eta \dot{M} c^2 \simeq 5.6 \times 10^{31} \mathrm{erg\,s^{-1}}. \tag{4.25}$$

Table 4.1: Accretion parameters for different black hole masses.

M_{BH} ($\mathrm{M}_\odot$)	r_B (pc)	$\dot{M}$ ($\mathrm{M}_\odot$ yr^{-1})	L_{acc} (erg s^{-1})
10^6	5.9×10^{-2}	1.04×10^{-7}	5.89×10^{38}
10^7	5.9×10^{-1}	1.04×10^{-5}	5.89×10^{40}
10^8	5.9	1.04×10^{-3}	5.89×10^{42}
10^9	5.9×10^{1}	1.04×10^{-1}	5.89×10^{44}

This represents only ~ 1.5 % of $L_\odot$.

Because the solution of equation (4.24) is for dimensionless variables, it can be applied to objects of any scale. We just need to select the parameters of the ISM and the mass of the BH. Here we apply the solution to super massive BHs, as those predicted in AGNs. Figure 4.3 displays the velocity profiles for different black hole masses, panels a, b, c and d present the results for $M_{BH} = 10^6 M_\odot$, $10^7 M_\odot$, $10^8 M_\odot$ and for $10^9 M_\odot$, respectively. In all cases an ISM whose gas number density is n=0.1 cm^{-3}, temperature T=10^6 K, and polytropic index $\gamma = 4/3$ was assumed. As one can see, the sonic radius, r_B, is a linear function of the black hole mass (see equation 4.10). The accretion rates and the accretion luminosities are presented in Table 5.1, these scale as the square of the black hole mass (see equation 4.21). The density and the temperature used for these calculations are typical of the ISM coronal phase.

4.3.1 Asymptotic limits.

In the region $r < r_B$, the gas moves supersonically and the inflow velocity asymptotically approaches the free fall value (see equation 4.17, for $u \gg c_s$):

$$u^2 \cong \frac{2GM}{r} = v_{ff}^2 \quad \text{for} \quad r \ll r_B, \tag{4.26}$$

where v_{ff} is the free fall velocity. Using the continuity equation (4.14) and the free fall velocity one can obtain

$$\rho \cong \frac{1}{2}\rho_B \left(\frac{r_B}{r}\right)^{3/2} \quad \text{for } r \ll r_B. \tag{4.27}$$

From the perfect gas law and the polytropic relation one can then estimate the temperature of the gas in the region inside the Bondi radius:

$$T \cong T(r_B) \left(\frac{r_B}{r}\right)^{3(\gamma-1)/2} \quad \text{for } r < r_B. \tag{4.28}$$

These equations (4.26 - 4.28) provide an analytic approximation to the gas parameters interior to r_B.

4.4 Accretion onto the super massive BH in the center of the galaxy M87.

The super massive black holes at the centers of elliptical galaxies are likely to accrete primarily from the surrounding hot, quasi-spherical ISM. The mass accretion rate can then be estimated using Bondi accretion theory that requires an accurate measurement of the gas parameters at the Bondi radius. Di Mateo et al. (2003) studied the accretion onto the supermassive black hole in M87 using Bondi accretion theory and X-ray observations from *Chandra*. The nucleus of the giant elliptical galaxy M87 contains a black hole whose mass, $M \sim 3 \times 10^9 M_\odot$, was determined from the *Hubble Space Telescope (HST)* observations (Ford et al. 1995; Harms et al. 1994; Macchetto et al. 1997). This galaxy has an active galactic nucleus. The temperature of the gas within the central kpc is $kT = 0.8$ keV. Di Mateo et al. (2003) found that within the central ~ 2 kpc the density profile flattens reaching a value of n_e=0.17 cm^{-3}. We use these values of temperature, density and mass of the black hole in our numerical scheme to derive parameters of the Bondi accretion flow. At the M87 distance (18

Mpc) the spatial resolution of *Chandra* corresponds to $\sim$ 100 pc. A crude estimation of the radius at which the gravitational energy balances the kinetic energy of a particle of mass m under the gravitational pull of the BH mass, M_{BH}, gives

$$r = \frac{2GM_{BH}}{u^2}. \tag{4.29}$$

Looking at equation (4.17), for larger r the gravitational pull of the accreting object is weak and all quantities have their 'ambient' values (ρ_{ISM}, c_{ISM}, $u \sim 0$). As one moves to smaller r the inflow velocity increases until u reaches the ISM sound speed, c_{ISM}. At this point, density and sound speed begin to increase above their ambient values. Then using equation (4.29) one can define an accretion radius, r_{acc}:

$$r_{acc} = \frac{2GM}{c^2_{ISM}} \simeq 150\,\mathrm{pc}, \tag{4.30}$$

where $c^2_{ISM} = \gamma k T_{ISM}/\mu$, T_{ISM} is the temperature of the hot ISM and $\mu = 14/23\, m_H$ is the mean mass per particle of the ionized ISM. Regions of such size can be resolved with *Chandra*.

Figure 4.4 shows the velocity profile and density distribution for the case of M87. Panel a, presents the inflow velocity derived from the numerical calculations (solid line) and its asymptotic limit (dotted line), $v_{ff} \propto r^{-1/2}$. Panel b, displays the density distribution that results from the numerical calculations (solid line) and its asymptotic value (dotted line), $\rho \propto r^{-3/2}$. The parameters used for M87 give us an ISM sound speed c_{ISM} = 409 km s^{-1}, which was used to calculate the Bondi radius, r_B = 19 pc, and the Bondi accretion rate $\dot{M}_B \sim 0.06 M\odot$ yr^{-1}. The luminosity associated with this accretion rate is

$$L_B = \eta \dot{M}_B c^2 \simeq 3 \times 10^{44} \mathrm{erg\,s^{-1}} \tag{4.31}$$

where we have used an accretion efficiency η = 0.1. Note that in this case the Eddington luminosity, $L_{Edd} \cong 1.3 \times 10^{38} \frac{M}{M_\odot}$ erg s^{-1}, is 3 orders of magnitude larger than the Bondi accretion luminosity, L_B. The derived values for the accretion radius,

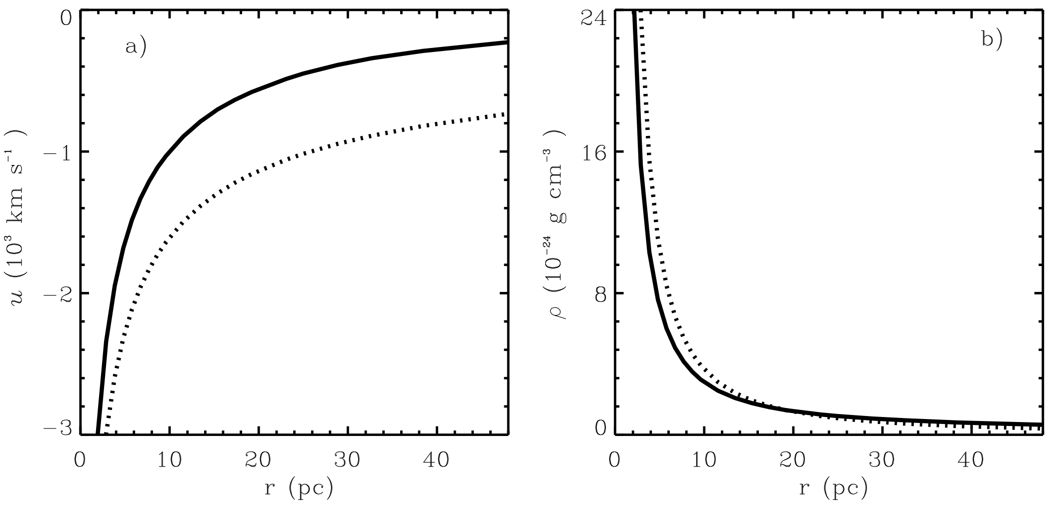

Figure 4.4: Bondi solution for the M87 galaxy. Panel a, displays the velocity (solid line) and the asymptotic approach (dotted line). Panel b, shows the density distribution (solid line) and the asymptotic approach (dotted line). The parameters are described in the text.

the accretion rate and the luminosity are in very good agreement with those obtained by Di Mateo et al. (2003).

The *Chandra* X-ray luminosity of the AGN in M87 is $L_{X,0.5-7\,keV} \sim 7 \times 10^{40}$ erg s^{-1}. It is at least 4 orders of magnitude smaller than the predicted Bondi luminosity. The low luminosity observed implies that the accretion efficiency is small or that the Bondi model is inappropriate in this case. In particular, a low radiative efficiency may result from strong outflows that may remove most of the mass and energy from the accretion flow (Blandford & Begelman, 1999; Stone et al. 1999). Di Mateo et al. (2003) suggested that adding the thermal energy provided by the jet into the energy conservation equation may reduce the accretion radius and, consequently, the accretion rate with respect to the Bondi value.

4.5 Conclusions

In this chapter we studied the inner structure of Bondi accretion flows. We presented a formal solution for the accretion problem. We proved that although there are many simplifications in the Bondi accretion physics, the broad picture seems to be correct, so this model should be regarded as a reference and can be used as a test for systems of different scales.

The key parameter in the spherically symmetric accretion theory is the accretion rate. It may be derived from the ambient conditions (ρ_{ISM} and T_{ISM}) of the ISM far away from the accreting body.

There is only one *transonic* solution for the spherically symmetric accretion, for which the gas moves with subsonic velocity outside the Bondi radius, reaches the sound speed at r_B, and then moves with supersonic velocity approaching a free fall velocity for $r \ll r_B$. The sonic radius, r_B, changes linearly with mass of the accreting black hole while the mass accretion rate changes as a square function of the BH mass.

The main shortcoming of Bondi theory is that it uses a very simplified polytropic gas law and does not include radiative losses of energy and the mass deposition from massive stars. An accurate model thus requires that the energy conservation equation must be used instead of equation (4.5). The comprehensive study of spherically symmetric accretion including radiative cooling and outflow effects is presented in the next chapter, where we develop a self-consistent theory of spherically symmetric accretion that takes into consideration both the energy and mass deposition from the stellar cluster around a central massive black hole.

Chapter 5

The impact of a black hole's gravity on the super star cluster wind radiative solution.

Abstract

Intensive studies of active galactic nuclei in several spectral ranges provide strong evidence for the presence of a massive starbursts around the central supermassive black hole, mainly in Seyfert galaxies (Heckman et al. 1997; González Delgado et al. 1998). The black hole mass vs velocity dispersion ($M_{BH} - \sigma$) relation (Greene & Ho 2006, and references therein) as well as the black hole mass vs bulge mass ($M_{BH} - M_{bulge}$) relation (Häring & Rix 2004, and their references) tell us also that black holes at the center of galaxies and the surrounding stellar systems are closely related. In this chapter we develop a self-consistent hydrodynamic model to study the internal structure and kinematics of the accretion flows and the starburst driven winds that result from stellar clusters with a super massive central black hole. We derive the hydrodynamic equations that take into consideration the gravitational pull of the star cluster and the central black hole *and then solve them numerically. We provide numerical calculations for 7 objects of different scales: 3 selected from the list of galaxies with central super massive black holes of Häring & Rix (2004), the globular cluster G1 and for 3 synthetic objects with an intermediate mass black hole. We propose a simple analytic approximation to the numerical mass accretion rate and to the position of the stagnation point. Finally, we briefly discuss the case when catastrophic cooling begins to dominate over gravity affecting the inner structure of the resulting flow.*

5.1 Introduction

Super massive black holes ($M_{BH} \sim 10^7 M_\odot - 10^{10} M_\odot$) are thought to be present in the centers of active galactic nuclei (AGNs). Intensive studies of AGNs in optic, infrared (IR) and X-ray regimes during the last decade provided also strong evidence for the presence of a massive starbursts around the central BH in a number of Seyfert galaxies.

For example, Rodríguez Espinosa et al. (1987) found from a sample of optically selected Seyfert galaxies that far-IR colors are indistinguishable from that of starbursts galaxies. They suggest then that far-IR luminosities associated with many Seyfert galaxies indicate on an intrinsic link between the circumnuclear star formation and the AGN activity.

Baum et al. (1993) found from a sample of Seyfert galaxies that the morphology of the diffuse radio emission, its intensity, correlation with the far-IR luminosity of the host galaxy and 25 - 60 μm spectral index are consistent with the heated dust emission and suggested that circumnuclear starbursts and starburts driven winds may be intrinsic for many Seyferts despite their relative strengths may vary from one to another galaxy.

Levenson et al. (2001) presented results of the X-ray imaging and spectroscopic

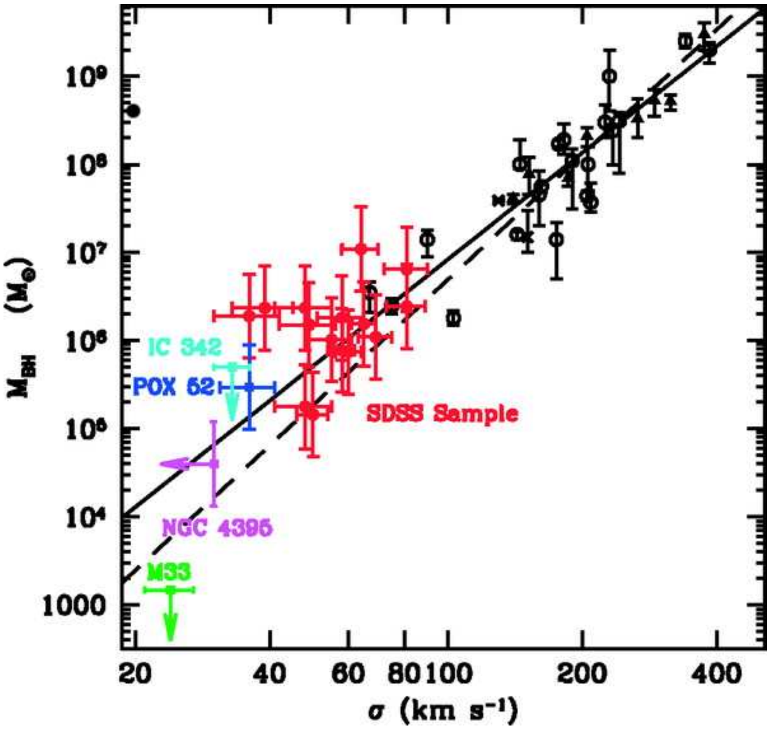

Figure 5.1: The $M_{BH} - \sigma$ relation (from Barth et al. 2005). The solid and dashed lines represent the $M_{BH} - \sigma$ relations derived by Tremaine et al. (2002) and Merritt & Ferrarese (2001), respectively. The black symbols are black holes compiled by Tremaine et al. (2002). In red a sample from the SDSS compiled by Barth et al. (2005). Other nearby galaxies are also indicated.

analysis of Seyfert 2 galaxies. They found that the X-ray spectra of their galaxies require, in addition to the power-law Seyfert component, a thermal emission with $kT = 0.8$keV which is characteristic of pure starburst. Jiménez-Bailón et al. (2005) presented results of the XMM-Newton and Chandra observations of the Seyfert 2 galaxy NGC 1808. They found that the hard X-ray emission is associated with the unresolved nuclear sources whereas the soft one is dominated by a thermal component associated with an extended starburst.

Heckman et al. (1997), González Delgado et al. (1998) presented a direct evidence for the existence of nuclear starbursts in the four Seyfert 2 galaxies Mrk 477, NGC 7130, NGC 5135 and IC 3639. They found in the UV and optical spectra of these galaxies the absorption line features associated with photospheres of O and B stars and their stellar winds. The nuclear in these galaxies have sizes from less than 100 pc to a few hundred parsecs. The co-existence of the W-R features in the optical and CaII triplet in the near-IR part of the spectra requires a continuous star formation during more than ~ 10 Myr or two stellar generations with the age of (5-6) Myr for the younger starburst and (10-20) Myr for the older one, respectively. Such starbursts are likely drive high-velocity outflows detected in the above and Seyfert 2/starburst composite ultraluminous infrared galaxies (González Delgado et al. 1998; Rupke et al. 2005).

On the other hand, the $M_{BH} \sim \sigma^4$ relation between the mass of the black hole and the velocity dispersion in the bulge of the host galaxy, revealed by Ferrarese & Merritt (2000), Merritt & Ferrarese (2001), Gebhardt et al. (2000), Tremaine et al. (2002), Greene & Ho (2006), can be extrapolated to intermediate-mass black holes (hereafter IMBH), see Figure 5.1, which shows that the $M_{BH} - \sigma$ relation extends over more than 4 orders of magnitude along the mass range (Barth et al. 2005). Recently it was also proposed that massive stellar clusters may host a central IMBH with mass about $M_{BH} \sim 10^3 - 10^6 M_\odot$ (see Barth et al. 2005; Gebhardt et al. 2005; Greene & Ho 2006). The globular cluster G1 in the M31 galaxy may be the best example of a cluster with an IMBH of mass $M_{BH} \sim 2 \times 10^4 M_\odot$ (Gebhardt et al. 2002, 2005; see however Baumgardt et al. 2003 and Pooley & Rappaport 2006, for an alternative scenario). These results between M_{BH} and σ as well as the correlation between the black hole mass and the bulge mass of the host galaxy, $M_{BH} - M_{bulge}$, (Merritt & Ferrarese 2001; Marconi et al. 2003; Häring & Rix 2004) indicate that black holes and the surrounding stellar systems are closely related.

The connection between a star forming galaxy and its nuclear activity has been suggested in several works, like for example Lípari & Terlevich (2006) and references therein. They proposed an evolutionary scenario where a super massive black hole is formed during the formation of the galactic core, resulting in an active nucleus powered by accretion of part of the mass reinserted by the massive members of a circumnuclear starburst onto the super massive black hole.

The starburst can dramatically alter the structure of the host galaxy. In fact, the combined action of supersonic stellar winds from young stars and supernova explosions promotes the formation of a hot X-ray emitting super bubble. This bubble expands and eventually breaks out to form a galactic or star cluster wind. The structure of a super stellar cluster wind is strongly affected when radiative cooling is considered (see Silich et al. 2004). As demonstrated by Silich et al. (2004) and corroborated by Tenorio-Tagle et al. (2007), there is a threshold line for the super stellar cluster's mechanical luminosity. This line separates clusters that are able to drive a stationary quasi-adiabatic or strongly radiative wind from those evolving in a bimodal regime in which catastrophic cooling in the central part of the cluster volume accumulates the injected matter, while the outer zones are still able to drive a stationary super wind (Tenorio-Tagle et al. 2007).

In this chapter we study the hydrodynamics of the gas inserted by massive stars and supernova explosions of a massive stellar cluster subjected to the influence of the gravity of a super massive black hole (BH) at the center. We consider a self-consistent radiative scenario by taking into account the mass and energy deposition from the stellar component, we also consider radiative losses. Section 5.2 presents the basics of the model: the main assumptions, simplifications and the input physics. Section 5.3 presents the main equations, the selected boundary conditions and the method of solution. In section 5.4 we apply our model to bulges of galaxies with central super massive black holes and to massive stellar clusters with IMBHs, we present the integral curves for the wind and the accretion flows as well as density and temperature distributions for the selected objects. There we propose an analytic approximation to the mass accretion rate and to the position of the stagnation radius. In section 5.5 we briefly discuss the case of stellar clusters above the threshold line. Section 5.6

summarizes our results and gives conclusions.

5.2 The model

A composite black hole - starburst system results in a variety of physical processes. However, here we concentrate on the influence of a black hole on the hydrodynamics of the matter injected by the massive members of the stellar cluster by making some assumptions and simplifications: first of all, we consider a static super massive black hole at the center of a spherically symmetric stellar cluster, we assume that the cluster has a large number of young massive stars and supernova explosions, distributed homogeneously throughout its volume. We suppose that the gas injected by massive stars and supernova explosions is completely thermalized due to random interactions between individual stellar winds and supernova ejecta. We take into account radiative losses. The heating efficiency and radiative pressure are neglected in our approach. We assume zero total angular momentum for the system.

5.2.1 Input physics

The gravitational well associated with the central BH results in the displacement of the stagnation radius, R_{st}, (the radius at which the gas velocity is zero) from the star cluster center towards the star cluster surface. Inside the stagnation radius the gravitational field of the central black hole dominates and the matter injected by stellar winds and supernova explosions is accreted onto the BH, despite a high thermal pressure provided by thermalization. On the other hand, outside of the stagnation radius the injected matter flows away forming a star cluster wind. Figure 5.2 shows an artistic representation of the model. The small circle shows the black hole's sphere of influence of radius R_{st} and the external circle or radius R_{sc} represents the star cluster surface. The central black dot marks the position of the black hole. The arrows directed towards the center represent the accreting gas whereas those

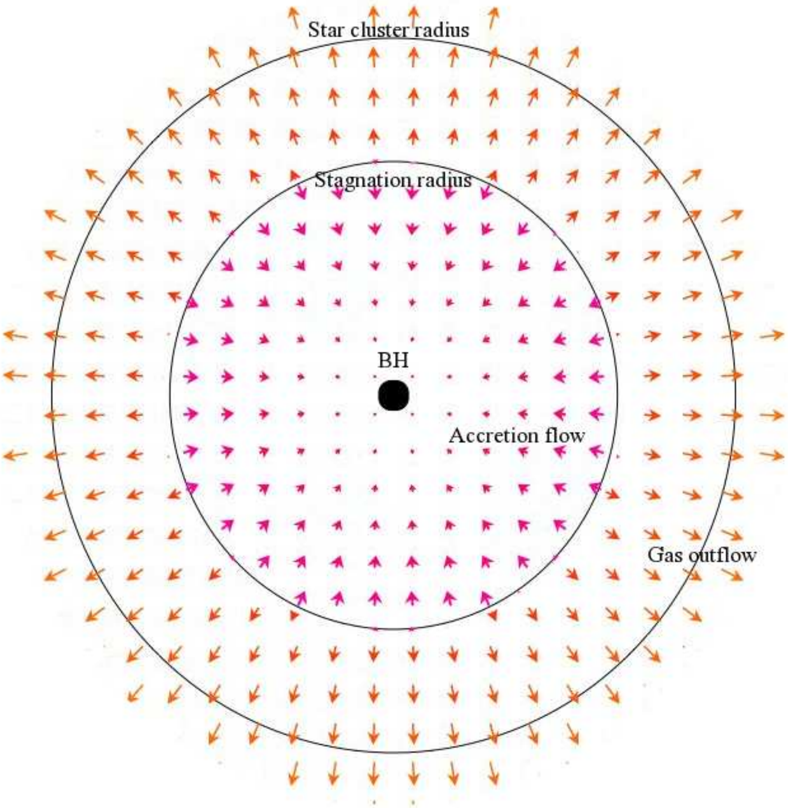

Figure 5.2: The structure of the flow that results from the thermalization of the supernova ejecta and stellar winds when a massive black hole is present at the star cluster center. The radii of the internal and the external circles represent the stagnation radius R_{st} and the star cluster radius R_{sc}, respectively. The arrows indicate the direction of the flow and the central dot shows the position of the black hole.

directed outwards represent the out-flowing matter.

5.3 Main equations and solution

To derive the equations of mass, momentum and energy conservation, we use newtonian physics. The set of equations that we use in this chapter are similar to those in Chapter 3, section 3.3, except for the terms which incorporate the gravity of the central BH. We solve the set of equations following the ideas proposed in Silich et al. (2004), Tenorio-Tagle et al. (2007) for three separate regions: 1) outside of the cluster, 2) between the star cluster radius and the stagnation radius and 3) inside the stagnation radius.

The set of hydrodynamic equations outside of the cluster

Outside of the cluster the equations of mass, momentum and energy conservation in spherical coordinates, are:

$$\frac{1}{r^2}\frac{d}{dr}\left(\rho_w u_w r^2\right) = 0, \tag{5.1}$$

$$\rho_w u_w \frac{du_u}{dr} = -\frac{dP_w}{dr} - \frac{G\rho_w(M_{BH} + M_{sc})}{r^2}, \tag{5.2}$$

$$\frac{1}{r^2}\frac{d}{dr}\left[\rho_w u_w r^2 \left(\frac{u_w^2}{2} + \frac{\gamma}{\gamma - 1}\frac{P_w}{\rho_w}\right)\right] = -Q - \frac{G\rho_w u_w(M_{BH} + M_{sc})}{r^2}. \tag{5.3}$$

As it was demonstrated in Chapter 3, equations (5.1)-(5.3) can be presented in a more convenient form:

$$\rho_w = \frac{\dot{M}_w}{4\pi u_w r^2}, \tag{5.4}$$

$$\frac{dP_w}{dr} = -\frac{\dot{M}_w}{4\pi r^2}\frac{du_w}{dr} - \frac{\rho_w G(M_{BH} + M_{sc})}{r^2}, \tag{5.5}$$

$$\frac{du_w}{dr} = \frac{(\gamma - 1)Q/\rho_w + 2u_w(c_s^2 - \frac{V_{esc}^2}{4})/r}{u_w^2 - c_s^2}, \tag{5.6}$$

where M_{BH} and M_{sc} are the black hole and the cluster mass, respectively. $c_s = (\gamma P_w/\rho_w)^{1/2}$ is the sound speed and $V_{esc}(r) = [2G(M_{BH} + M_{sc})/r]^{1/2}$, is the escape velocity at radius r. The mass returned by the star cluster into the interstellar medium is equal to the total mass deposited by supernova explosions and stellar winds, $\dot{M}_{sc}$, minus that injected within the stagnation radius, $\dot{M}_{st} = \dot{M}_{sc}\,(R_{st}/R_{sc})^3$: $\dot{M}_w = \dot{M}_{sc}\,(1 - R_{st}^3/R_{sc}^3)$

The set of hydrodynamic equations inside the cluster

Inside the cluster the main hydrodynamic equations are:

$$\frac{1}{r^2}\frac{d}{dr}\left(\rho_w u_w r^2\right) = q_m, \tag{5.7}$$

$$\rho_w u_w \frac{du_w}{dr} = -\frac{dP_w}{dr} - q_m u_w - \frac{G\rho_w(M_{BH} + M(r))}{r^2}, \tag{5.8}$$

$$\frac{1}{r^2}\frac{d}{dr}\left[\rho_w u_w r^2 \left(\frac{u_w^2}{2} + \frac{\gamma}{\gamma - 1}\frac{P_w}{\rho_w}\right)\right] = q_e - Q - \frac{G\rho_w u_w(M_{BH} + M(r))}{r^2}, \tag{5.9}$$

where $M(r)$ is the mass of the stellar system as a function of r. In the case of a homogeneous stellar mass distribution, the mass within a spherical volume of radius r is $M(r) = M_{sc}(r/R_{sc})^3$.

For $r \leq R_{sc}$, the constant C in the integral form of the mass conservation equation, is not equal to zero:

$$\rho_w = \frac{q_m r}{3u_w} + \frac{C}{u_w r^2}. \tag{5.10}$$

The value of C depends on the location of the stagnation point, $C = -q_m R_{st}^3/3$, and thus the mass conservation equation (5.7) is

$$\rho_w = \frac{q_m r}{3u_w}\left(1 - \frac{R_{st}^3}{r^3}\right). \tag{5.11}$$

Using this equation one can replace terms $\rho_w u_w$ and $\rho_w u_w r^2$ in equations (5.8) and (5.9). Taking the derivative in equation (5.9) and replacing dP_w/dr from equation (5.8), we obtain:

$$\frac{du_w}{dr} = \frac{1}{\rho_w}\frac{(\gamma - 1)(q_e - Q) + q_m\left[\frac{(\gamma+1)}{2}u_w^2 - \frac{2}{3}\left(1 - \frac{R_{st}^3}{r^3}\right)\left(c_s^2 - \frac{V_{esc}^2}{4}\right)\right]}{c_s^2 - u_w^2}, \tag{5.12}$$

$$\frac{dP_w}{dr} = -q_w\left[\frac{r}{3}\left(1 - \frac{R_{st}^3}{r^3}\right)\frac{du_w}{dr} + u_w\right] - \frac{G\rho_w(M_{BH} + M(r))}{r^2}, \tag{5.13}$$

where the escape velocity is $V_{esc} = [2G(M_{BH} + M(r))/r]^{1/2}$. Equations (5.11)-(5.13) describe the flow inside the cluster, for both regions: between the stagnation radius, R_{st}, and the edge of the cluster, R_{sc}, and also in the region $r \leq R_{st}$, where the injected matter accretes onto the central black hole.

5.3.1 Boundary conditions and solutions.

As was shown by Silich et al. (2004) and in Chapter 3, section 3.3. For clusters below the threshold line one can always select the proper central temperature that places the sonic point at the cluster surface (hereafter we refer to this sonic point as the *outer* sonic point), producing a stationary wind. When the black hole is considered, the stagnation point moves out of the center towards the cluster surface, introducing a second sonic point (hereafter we refer to this sonic point as the *inner* sonic point) interior to the stagnation radius. Thus the problem one has to solve in order to build a self-consistent solution is to find the proper position of the stagnation radius. In this respect, the proper position of R_{st} is defined by the second sonic point (which is similar to that in the Bondi accretion case with $\gamma = 5/3$), specifically that the *inner* sonic point ought to be at the star cluster center, see Eqs. (4.18) and (4.10). Here we replace this condition with

$$R_{sonic\ 2} = 3R_{Schw}, \tag{5.14}$$

where $R_{Schw} = 2GM_{BH}/c^2$ is the central black hole Schwarzschild radius, c is the speed of light and $3R_{Schw}$ is the radius of the last stable orbit around the black hole (see Frank et al. 2002). Smaller radii than $3R_{Schw}$ are not considered in our approach.

Like in the case without gravity, to carry out the numerical integration of equations (5.4-5.6) and (5.11-5.13), we need to know the relation between the gas number density, n_{st}, and temperature, T_{st}, at the stagnation radius. As shown in Appendix D, gravity does not change the relation between n_{st} and T_{st} with respect to that found by Silich et al. (2004) (see section 3.3):

$$n_{st} = q_m^{1/2} \left[\frac{V_{A,\infty}^2/2 - c_{st}^2/(\gamma - 1)}{\Lambda(Z, T_{st})} \right]^{1/2} \tag{5.15}$$

where, c_{st} is the sound speed at R_{st}, $V_{A,\infty} = (2q_e/q_m)^{1/2}$ is the adiabatic wind terminal speed.

Thus one can always select the T_{st} that sets the *outer* sonic point at the star cluster surface. Then we can use this temperature and the gas number density derived from equation (5.15) as initial conditions for the inward integration from R_{st} towards the star cluster center. The shape of the integral curves (see Figure 5.3) depend, however, on the location of the stagnation radius. If the selected R_{st} is too large, the backward integration leads to a double-valued, unphysical solution (see Figure 5.3, green line). In this case the turnoff point coincides with the second (*inner*) sonic point. The second sonic point moves towards the center when R_{st} becomes smaller and continuously approaches $3R_{Schw}$ (see Figure 5.4, panel c) to finally reach $3R_{Schw}$ for a certain value of R_{st}. For this stagnation radius the stationary solution sets in (see Figure 5.3, black line). For even smaller R_{st} the velocity of the flow inside R_{st} remains subsonic and may go to zero (see Figure 5.3, red line).

There is a family of integral curves whose R_{st} sets the inner sonic points at $r < 3R_{Schw}$ (see Figure 5.4, panel a). We select the largest R_{st}, that satisfies the condition (5.14). We select the largest R_{st} also because in this case the density at the stagnation point, ρ_{st}, is the smallest one (see Figure 5.4, panel d) required for a stationary accretion flow.

Then, the procedure that allows one to find the self-consistent hydrodynamic solution for the case of a star cluster with a central massive black hole is:

1. Select an arbitrary stagnation radius inside the cluster and iterate T_{st} until the *outer* sonic point sits at the star cluster surface.

2. Then, the selected ρ_{st} and T_{st} are used as initial conditions to integrate equations (5.11)-(5.13) inwards from the stagnation point.

3. If the integral curve has a transition from subsonic to supersonic velocities but is double valued, we select a smaller value for R_{st} and repeat the calculations.

4. We select the largest R_{st} from the condition that the *inner* sonic point sets at $3R_{Schw}$, with the minimum density required for a stationary solution.

Figure 5.4 shows different types of the integral curves that appear when one applies the above procedure. This plot results from an artificial, compact $R_{sc} = 3$ pc cluster with mass $M_{sc} = 5 \times 10^5 M_{\odot}$, with the same mass for the central BH.

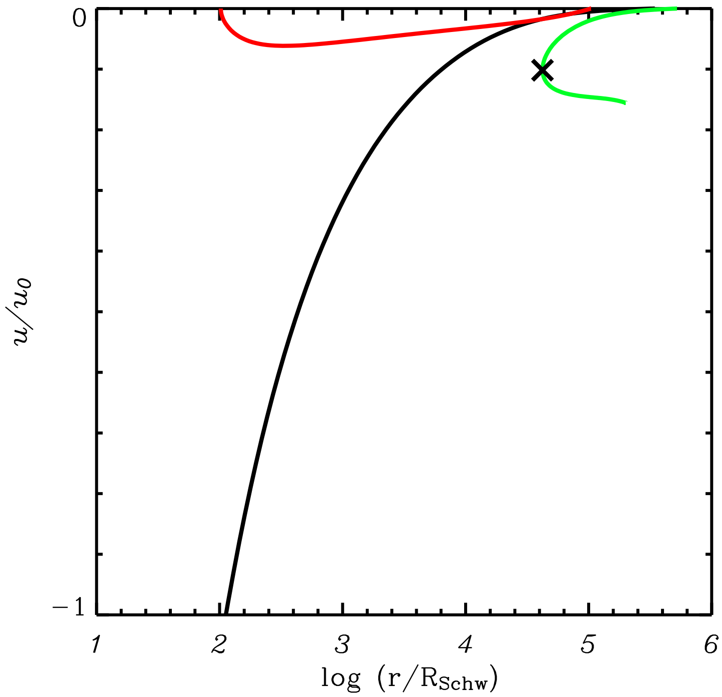

Figure 5.3: Possible types of the integral curves inside R_{st}. Three possible integral curves marked by green, black and red lines correspond to three different positions of the stagnation radius: 1 pc, 3.3 pc and 5 pc, respectively. Green line represents a transonic unphysical solution whose sonic point marked by a cross coincides with the turnoff of the line. Red line displays a mathematical everywhere subsonic solution. We select the black line as the proper solution because it satisfies the boundary conditions for the *inner* and the *outer* sonic points and has the smallest density at the stagnation point, and allows also a smooth solution with a positive du/dr across the flow. The normalization velocity, $u_0 = 10^4$km s^{-1}, for black and green lines, and $u_0 = 10^2$km s^{-1} for the red line. These solutions were derived from an artificial system with $M_{sc} = M_{BH} = 10^8 M_\odot$, radius, 100 pc, and the adiabatic wind terminal speed, $V_{A,\infty} = 1500$km s^{-1}. It was assumed that the metallicity of the plasma is solar.

Panel a, shows the integral curves for the region $R_{st} \leq r \leq R_{sc}$, obtained for different stagnation radii. All these solutions have the *outer* sonic point at the star cluster

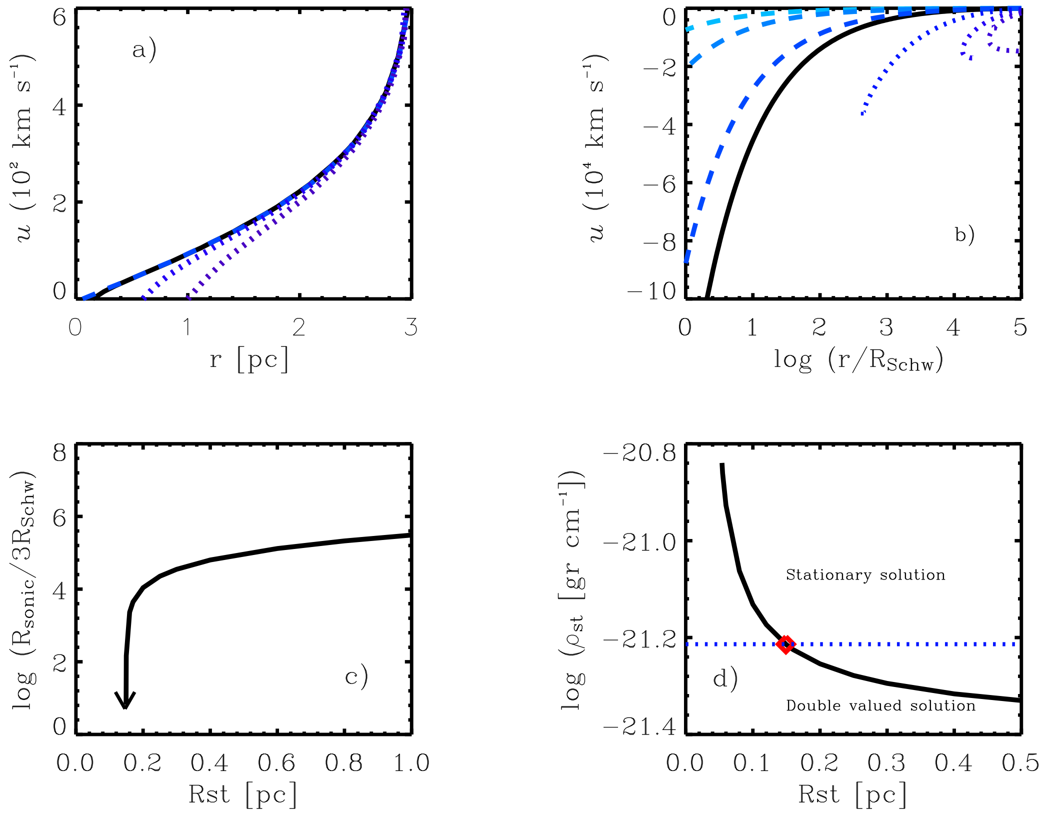

Figure 5.4: The family of integral curves for a $R_{sc} = 3$ pc cluster with mass $M_{sc} = 5 \times 10^6 M_\odot$ and $V_{A,\infty} = 1500$km s^{-1}. We have considered $M_{BH} = 5 \times 10^6 M_\odot$. Solar metallicity was assumed in all calculations. Panels a and b display the shape of integral curves for different positions of the stagnation point. Panel c, shows how the sonic point moves towards the center for different values of R_{st}. Panel d, displays the density at the stagnation point, ρ_{st}, as a function of R_{st}. All these curves are described in the text.

surface. The black solid line represents the selected proper solution whose R_{st} sits the *inner* sonic point at $r = 3R_{Schw}$. Panel b, displays the integral curves for $r \leq R_{st}$. The solid line represents the proper solution (i.e, is the continuation of the solid line in panel a) which satisfies both boundary conditions: the outer sonic point sits at the star cluster surface (see panel a) and the inner one is at $r = 3R_{Schw}$ (see panel c). In this case the density at R_{st} is the smallest (see panel d) between those allowed by the stationary solutions with positive derivatives, $du/dr > 0$, everywhere in the flow. Dotted lines in panel b are unphysical solutions whose sonic points coincide with their turn-off points. Dashed lines in panel b satisfy the external boundary condition but not the internal one.

Panel c, shows how the sonic point approaches the last stable orbit, $3R_{Schw}$, when the stagnation radius moves towards the appropriate R_{st}. Panel d displays ρ_{st} as a function of R_{st}. The red diamond marks the density associated with the selected proper solution. Note that only unphysical double-valued solutions result from a smaller ρ_{st}. The horizontal line separates the double-valued solutions (below the line) from the single valued ones (above the line).

Thus, there is a number of integral curves for our main equations (5.4)-(5.6) and (5.11)-(5.13). However, there is only one solution that simultaneously satisfies the two boundary conditions: the outer sonic point is at the star cluster surface and the inner one is at $r = 3R_{Schw}$. We select this solution as the proper physical self-consistent solution.

5.4 Application to galaxies with a central super massive black hole

In the previous section, we found the stationary solution for fictitious objects, in the sense that we have used an arbitrary mass for the BH. In reality, the mass of the BH is just a small fraction of the mass of the stellar component. $M_{BH} \sim 10^{-3} M_{bulge}$, according to Merritt & Ferrarese (2001). Hereafter, we use the terms stellar cluster and bulge without distinction, as both refer to the stellar component.

The main condition on the stellar cluster to apply our model is that its mechanical luminosity must be below the threshold energy (see Chapter 3, section 3.3). But the position of the threshold line strongly depends on metallicity and also on the assumed adiabatic wind terminal speed (see Rodríguez-González, 2006). Here, we standarize all cases to solar metallicity, $Z_\odot$, and to $V_{A,\infty} = 1500$ km s^{-1} for the adiabatic wind terminal speed, which is a typical wind velocity in the starburst model of Leitherer et al. (1999). In all cases, the star cluster mechanical luminosity, $L_{sc} = \dot{M}_{sc}V_\infty^2/2$, is assumed to be constant and scaled linearly with the mass of the cluster: $L_{sc} = L_{LH}(M_{sc}/M_{LH})$, where the L_{sc} has been normalized to the standard model $M_{LH} = 10^6 M_\odot \longrightarrow L_{LH} = 3 \times 10^{40}$ erg s^{-1}, of Leitherer & Heckman (1995).

Once we have made the above simplifications, to apply our model we just need 3 physical parameters: the mass of the stellar cluster, M_{sc}, its radius, R_{sc}, and the mass of the black hole, M_{BH}. We select and apply our model to several bulges of galaxies which have central massive black holes, from the list of Häring & Rix (2004). The model is also applied to the globular cluster G1, assuming that those stellar systems were formed instantaneously. Obviously all those objects are not young starburst since they are Gyr old, and probably do not have a sufficient number of stellar winds and SNe to completely thermalize the injected gas. We can, however, apply our model by using their parameters together with the assumptions given above. In fact, our model can be applied to starbursts - AGN galaxies, such as those mentioned in Lípari & Terlevich (2006), if they fulfill the requirements of our model.

The input data for the selected objects are plotted in Figure 5.5, panel a, which shows a tight correlation between the mass of the central black hole and the mass of the surrounding spheroid or bulge (see Häring & Rix, 2004):

$$\log\left(\frac{M_{BH}}{M_\odot}\right) = (8.20 \pm 0.10) + (1.12 \pm 0.06)\ \log\left(\frac{M_{bulge}}{10^{11} M_\odot}\right). \tag{5.16}$$

To derive the radius of the bulge we suppose that it is in virial equilibrium, then we use the velocity dispersion given by Häring & Rix (2004) and the relation:

$$M_{sc} = 7.5\frac{\sigma^2 r_m}{G} \tag{5.17}$$

where it is assumed that the cluster is spherically symmetric and has an isotropic velocity dispersion (see for example, Smith & Gallager 2001). We associated the

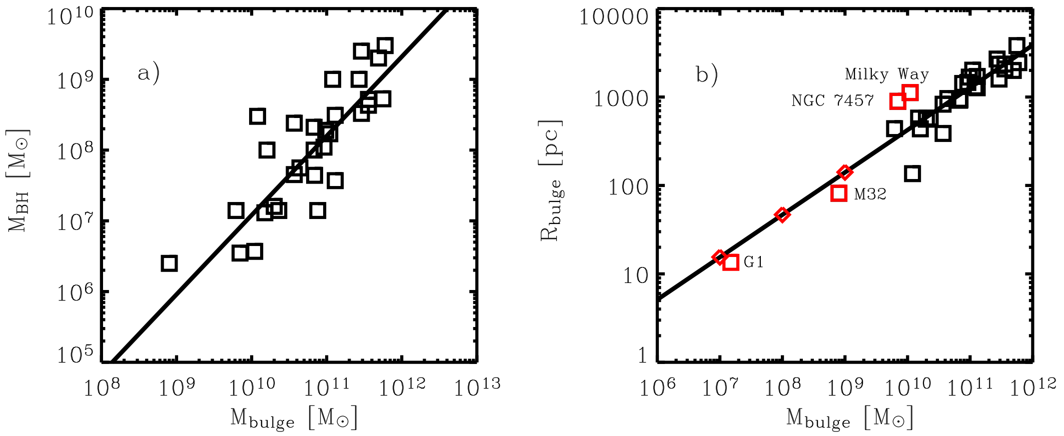

Figure 5.5: The $M_{BH} - M_{bulge}$ relation (panel a) from Häring & Rix (2004) and the derived $R_{bulge} - M_{bulge}$ relation (panel b). The red symbols are objects for which we apply our model. Red diamonds are artificial objects.

bulge radius with the half mass radius r_m, where $r_m = 4r_{hl}/3$, and r_{hl} is the half-light radius (see e.g. the review of Gerhard 2000).

Figure 5.5 Panel b displays the derived radii of the bulges against their masses for 30 objects from the list of Häring & Rix (2004). The red squares mark the objects for which we apply our model. A log-linear regression fit to Häring & Rix (2004) data results in

$$\log\left(\frac{R_{bulge}}{\mathrm{pc}}\right) = 0.48\ \log\left(\frac{M_{bulge}}{M_\odot}\right) - 2.17. \tag{5.18}$$

Extrapolating expression (5.18) to masses typical of massive star clusters we found that the fit is in good agreement with the data of the globular cluster G1, taken from Pooley & Rappaport (2006). Red diamonds in Figure 5.5b are artificial objects on the regression line (Eq. 5.18).

To select the appropriate objects we use the analytic approximation to the threshold line found in Wünsch et al. (2007), for the assumed $Z_\odot$ and $V_{A,\infty} = 1500$ km s^{-1} (see Figure 5.6). We found that most of the objects from the list of Häring & Rix (2004) evolve in the bimodal, catastrophic cooling regime (see Tenorio-Tagle et al.

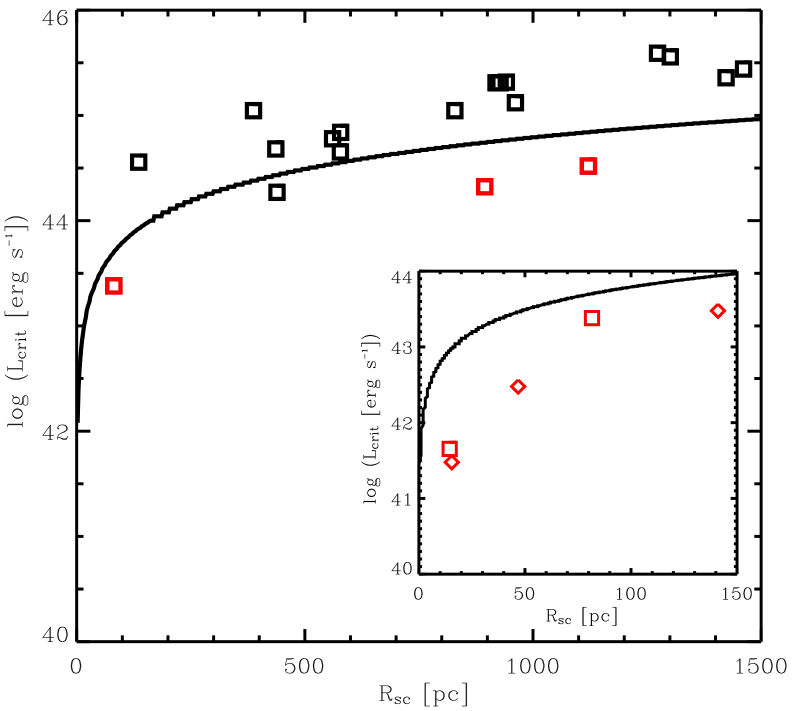

Figure 5.6: The star cluster mechanical luminosity - star cluster radius parameter space. The solid line marks the threshold luminosity (see Wünsch et al. 2007). The squares are objects from Häring & Rix (2004); the red symbols mark the selected objects which evolve in the sub-critical regime. From left to the right these are the bulges of M32, NGC 7457 and the bulge of the Milky Way. Squares in the insert are the globular cluster G1 and the bulge of M32, diamonds corresponds to artificial objects selected in Figure 5.5.

2007). Only three bulges from the list of Häring & Rix (2004) satisfy the condition for the mechanical luminosity (see Figure 5.6); these are the bulges of (from left to right in Figure 5.6): M32, NGC 7457, and the bulge of the Milky Way. The black square below the threshold line corresponds to the bulge of NGC 4742, excluded because it lays on the threshold in the numerical calculations. The red diamonds in the insert of Figure 5.6 corresponds to those in panel b (Figure 5.5), squares mark the bulge of M32 and the globular cluster G1 in M31 which is the best example of a globular cluster with an intermediate mass black hole $M_{BH} = 2 \times 10^4 M_\odot$ (see Gebhardt et al.

Table 5.1: Summary of object properties

Object (1)	M_{BH} ($M_{\odot}$) (2)	Ref. (3)	σ (km s^{-1}) (4)	M_{bulge} ($M_{\odot}$) (5)	Ref. (6)	L_{sc} (erg s^{-1}) (7)	R_{bulge} (pc) (8)	R_{st} (pc) (9)
SC1	5.3×10^3	...	...	1.0×10^7	...	3.0×10^{41}	15.5	2.0×10^{-3}
SC2	6.4×10^4	...	...	1.0×10^8	...	3.0×10^{42}	46.8	1.5×10^{-2}
SC3	9.0×10^5	...	...	1.0×10^9	...	3.0×10^{43}	141	1.5×10^{-1}
G1	2.0×10^4	1	...	1.5×10^7	7	4.5×10^{41}	13.5	5.0×10^{-3}
M32	2.5×10^6	2	75	8.0×10^8	5	2.4×10^{43}	81.6	2.8×10^{-1}
NGC 7457	3.5×10^6	3	67	7.0×10^9	3	2.1×10^{44}	894	7.3×10^{-1}
Milky Way	3.7×10^6	4	75	1.1×10^{10}	6	3.3×10^{44}	1120	8.5×10^{-1}

NOTE. —Col. (1): Object name. Col. (2): Black hole mass. Col. (3): References for the black hole mass. Col. (4): Stellar velocity dispersion from Tremaine et al. (2002), except for G1 which is taken from Meyland et al. (2001). Col. (5): Bulge mass. Col. (6) References for the photometric and kinematic data used for the adopted bulge mass. Col. (7): Mechanical luminosity scaled according with Leitherer & Hechman (1995). Col. (8): Bulge radius. Col. (9): Stagnation point for the self-consistent solution.

REFRENCES. —(1) Gebhadt et al. (2005); (2) Verolme et al. 2002; (3) Gebhardt et al. 2003; (4) Schödel et al. 2002; (5) Magorrian et al. 1998; (6) Bissantz et al. 1997; (7) Meyland et al. 2001.

2005).

The properties of the selected objects are summarized in Table 5.1. The clusters SC1, SC2 and SC3 are artificial objects represented by red diamonds in Figure 5.5 panel b, and in the insert in Figure 5.6. The BH masses in these cases were derived from relation (5.16) and the star cluster radii were calculated from equation (5.18). The mass of the globular cluster G1 and its central BH were taken from the literature (see references in Table 5.1), the cluster radius, $R_{G1} = 13.5$pc, was derived assuming a distance of 770 kpc (Freedman et al. 2001). The masses of the BHs and bulge mass in M32, NGC 7457 and the Milky Way have been taken from Häring & Rix (2004). Their radii were derived from the relation (5.17), where we used the stellar velocity dispersion from Tremaine et al. (2002). The mechanical luminosities in all cases were assumed to be constant and scaled linearly with the mass of the cluster (see Leitherer & Heckman, 1995).

From our numerical calculations we found that the cooling rate is not so impor-

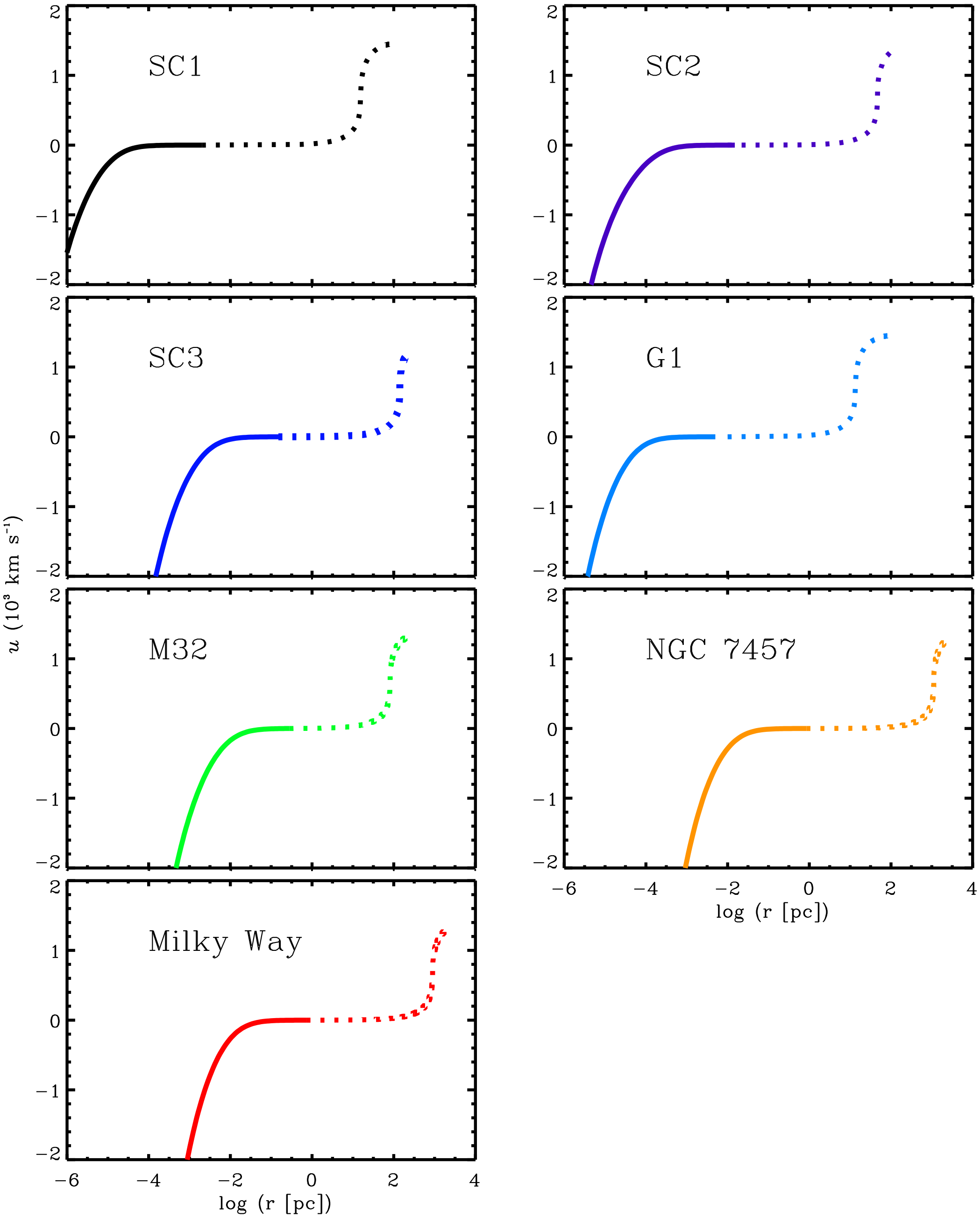
SC1
SC2
SC3
G1
M32
NGC 7457
Milky Way
u (10^3 km s^{-1})
log (r [pc])
log (r [pc])
2
1
0
−1
−2
−6
−4
−2
0
2
4

Figure 5.7a.—

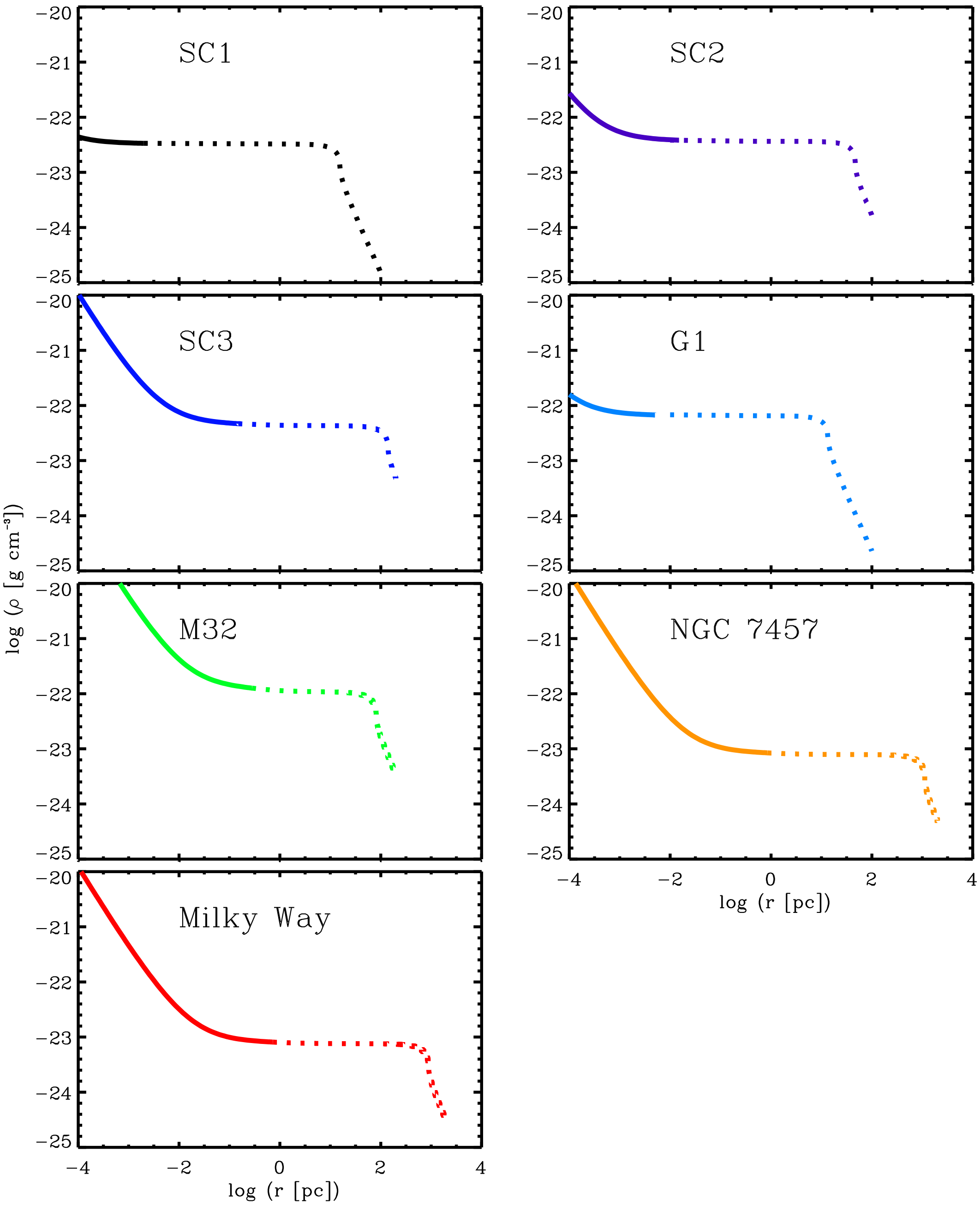
SC1
SC2
SC3
G1
M32
NGC 7457
Milky Way
log (ρ [g cm⁻³])
log (r [pc])
−20
−21
−22
−23
−24
−25
−4
−2
0
2
4

Figure 5.7b.—

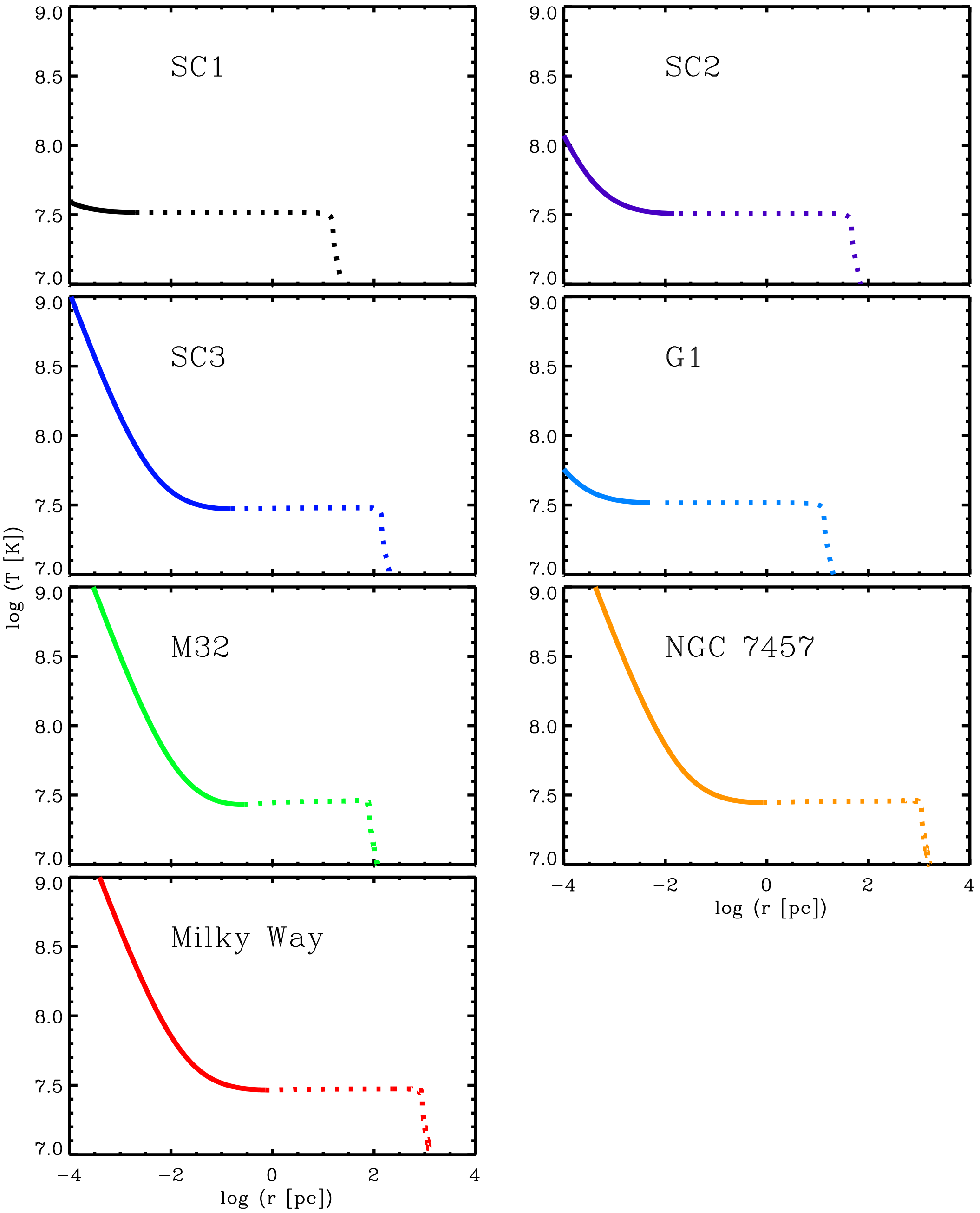

Figure 5.7c.—

Figure 5.7: The velocity integral curves and the distributions of density and temperature, panels a, b, and c, respectively, for a set of selected objects of different scales (see Table 5.1). Solid lines represent the accretion solution, while dotted lines represent the wind solution.

tant for the accretion flow and the gas accretes in a quasi-adiabatic regime, in contrast with the outflows where radiative cooling drastically modifies the temperature distribution. The shapes of the integral curves for all selected objects are shown in Figure 5.7. Panels a, b and c display the velocity, density and temperature, respectively, as functions of the distance to the center, r. Dotted lines represent the wind solution ($r \geq R_{st}$) and solid lines represent the accretion solution ($r \leq R_{st}$). Panel a, shows that for any stellar system below the threshold line we can always select the proper R_{st} to obtain a smooth, stationary solution for the hydrodynamics of the gas inserted by the stellar cluster under the gravitational field of a central BH. We found that for $r > R_{st}$ the gravity of the black hole does not affect significantly the shape of the wind solution. Note that in more massive BHs cases the gas accelerates more rapidly towards the center, as it is expected. Note also that for the range of BH masses here used, the stagnation radii are smaller than 1 pc. Panel b shows how density increases inside the stagnation radius. Observe that, inside R_{st}, density increases faster for larger BH masses, however, when we compare the density profile of M32 with that of the Milky Way, we observe the opposite, this is because the bulge of M32 is more compact and the ratio M_{sc}/R_{bulge}^3 is larger than in the Milky Way. Panel c shows how the gas temperature grows as it moves from R_{st} towards the BH. Note that, in some cases, the temperature is too high ($> 10^8$ K) in the central region leading possibly to X-rays.

5.4.1 An analytic approximation to the mass accretion rate and the stagnation radius

In the spherically symmetric case, all mass deposited by stellar activity within the volume delimited by the stagnation radius is accreted by the central black hole. However, it is known that even a small initial angular momentum would lead to the formation of an accretion disk around the black hole. In this way, the mass accretion rate calculated under assumption of spherical-symmetry should be considered as the upper limit to the mass accreted by the central object. In this respect, it is instructive to compare our theory (where M_{acc} represents a fraction of the total mass deposited by the stellar cluster, $\dot{M}_{sc}$)

$$\dot{M}_{acc} = \dot{M}_{sc} \left(\frac{R_{st}}{R_{sc}} \right)^3 \tag{5.19}$$

with Bondi's (Bondi 1952; Frank et al. 2002 and references therein) spherically symmetric accretion onto a black hole embedded in a homogeneous, static ISM:

$$\dot{M}_B = \pi G^2 M_{BH}^2 \frac{\rho_{ISM}}{c_{ISM}^3}, \tag{5.20}$$

where $\dot{M}_B$ is the Bondi accretion rate for an interstellar medium with polytropic index $\gamma = 5/3$ (see Appendix C), ρ_{ISM} and c_{ISM} are the density of the ISM and the sound speed at infinity. As below the threshold line (see section 3.3 in Chapter 3), density and temperature inside the cluster remain close to that derived from the adiabatic solution of Chevalier & Clegg (1985), see Silich et al. (2004). We can compare our results with those of a Bondi accretion by using the central temperature, T_c, and the central density, ρ_c, of a cluster evolving in the adiabatic regime (see Cantó & Raga, 2000):

$$\rho_c = \frac{1}{2\pi A} \frac{L_{sc}}{R_{sc}^2 V_{A,\infty}^3}, \tag{5.21}$$

$$T_c = \frac{\gamma - 1}{\gamma} \frac{\mu}{k} \frac{q_e}{q_m}, \tag{5.22}$$

$$c_c = \sqrt{\frac{\gamma - 1}{2}} V_{A,\infty}, \tag{5.23}$$

where the constant A corresponds to the relation (3.8) in Chapter 3, section 3.2.

The results of the comparison for the objects listed in Table 5.1 are shown in Figure 5.8, where our results (Eq. 5.19) are labeled by red diamonds. The solid line mark the Bondi accretion rates (Eq. 5.20) calculated under the assumption that ρ_{ISM} and c_{ISM} correspond to the central density ρ_c and sound speed c_c of an adiabatic star

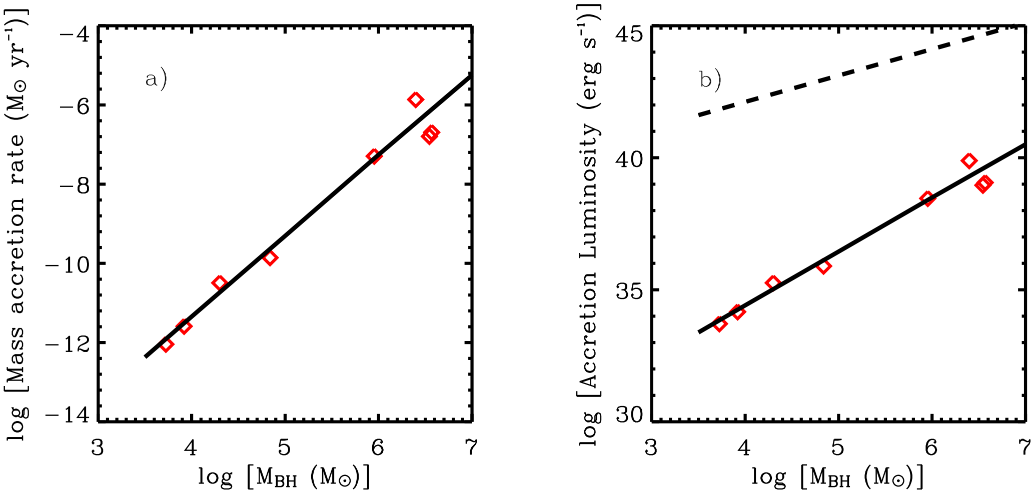

Figure 5.8: The accretion rates and accretion luminosities calculated for objects listed in Table 5.1. Red diamonds present the results of our numerical calculations. Solid line represents the analytic approximation to the numerical $\dot{M}_{acc}$, based on Bondi and Cantó et al., results. Dashed line represents the Eddington luminosity.

cluster wind. Figure 5.8 shows that one can reproduce our numerical results with a good accuracy if one uses Bondi's accretion theory (Eq. 5.20) with $\rho_{ISM} \approx \rho_c$ and $c_{ISM} \approx c_c$ derived from the adiabatic star cluster wind theory of Chevalier & Clegg (1985), see formulae (5.21) - (5.23).

The luminosity that results from the calculated mass accretion rates for an accretion efficiency $\eta = 0.1$, remains always below the Eddington limit $L_{Edd} \simeq 1.3 \times 10^{38} M_{BH}/M_{\odot}$ erg s^{-1} (see Figure 5.8b, where dashed line represents the Eddington luminosity and, red diamonds are the numerical results and solid line is the analytic approximation.

Because $M_{acc} \approx M_B$, we can derive an analytical formula for the mass accretion rate and for R_{st} in terms of the BH and the cluster parameters. Indeed, equating $M_{acc} \approx M_B$ (Eqs. 5.19 and 5.20) under the assumption that $\rho_{ISM} = \rho_c$, $c_{ISM} = c_c$:

$$\dot{M}_{acc} = \pi G^2 M_{BH}^2 \frac{\rho_c}{c_c^3}, \tag{5.24}$$

and taking into account that the mass deposition per unit volume is

$$q_m = \frac{3}{4\pi}\frac{\dot{M}_{sc}}{R_{sc}^3} = \frac{3}{2\pi}\frac{L_{sc}}{V_{A,\infty}^2 R_{sc}^3}, \tag{5.25}$$

one can obtain:

$$R_{st} = c_c\left(\frac{3}{4}\frac{G^2 M_{BH}^2 \rho_c}{q_m}\right)^{1/3}. \tag{5.26}$$

Thus below the threshold line one can obtain R_{st} from equation (5.26) if the cluster radius, the adiabatic wind terminal speed and the mass of the central black hole are known.

5.5 Stellar clusters in a catastrophic cooling regime

The theory developed in previous sections was applied to the case of clusters below the threshold line in the $L_{sc} - R_{sc}$ parameter space (see Chapter 3). Above the threshold line clusters evolve in a bimodal regime (see Tenorio-Tagle et al. 2007). In this regime, strong radiative cooling causes the displacement of the stagnation point from the center and leads to the accumulation of the mass injected inside the stagnation radius, while the outer zones drive a stationary outflow. As we show in Appendix D, the relation between the gas number density and the temperature at the stagnation point is not affected by gravity. One can then calculate the pressure at the stagnation point (see Figure 5.9) for any cluster from the relation:

$$P_{st} = kT_{st}q_m^{1/2}\left[\frac{V_{A,\infty}^2/2 - c_{st}^2/(\gamma-1)}{\Lambda(Z,T_{st})}\right]^{1/2}. \tag{5.27}$$

Figure 5.9 displays the relation between pressure and temperature at the stagnation point for clusters with different mechanical luminosities and radii 100 pc. For an energy input rate $L_{sc} = 3 \times 10^{42}$ (short-dashed line), the pressure at the stagnation point, which sets the sonic point at the star cluster surface, is smaller than the maximum pressure, P_{max}, which is associated with the critical temperature T_{crit}. Note, however that P_{st} becomes larger for more massive clusters (long-dashed line),

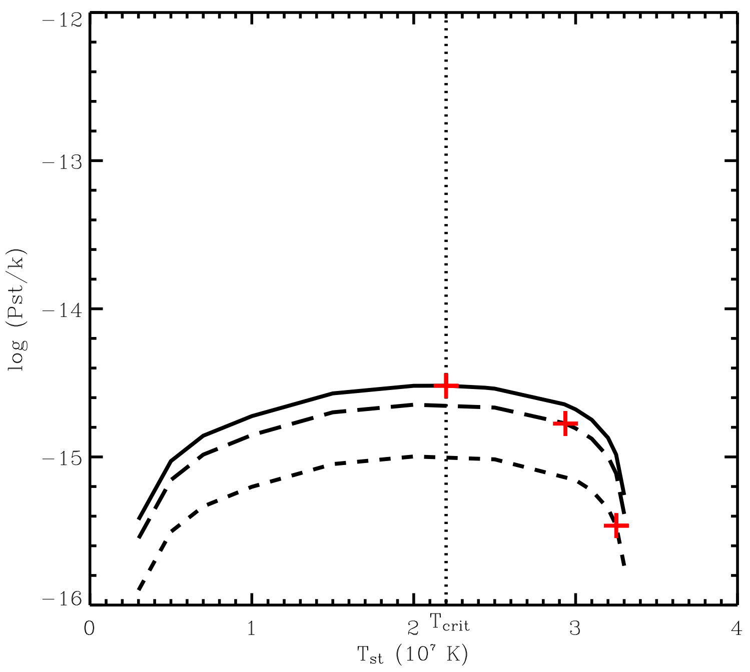

Figure 5.9: The pressure and temperature at the stagnation point for 100 pc clusters with different masses. The pressure at the stagnation point, P_{st}, for several clusters is indicated by the red crosses. P_{st} remains below the maximum possible value for clusters that are below the threshold line (the short and long-dashed lines), and acquires the maximum value, P_{max}, when $M_{sc} = M_{crit}$ (solid line). Note that P_{max} selects the critical stagnation temperature, T_{crit}, marked by the vertical line (see Tenorio-Tagle et al. 2007). $T_{crit} \approx 2.2 \times 10^7$ K for an assumed value of the adiabatic terminal speed $V_{A,\infty} = 1500$ km s^{-1}. Solid line represents the case with a critical energy input rate, $L_{sc} = 2.7 \times 10^{43}$ erg s^{-1}. Long-dashed and short-dashed are for clusters below the threshold line, with $L_{sc} = 1.5 \times 10^{43}$ and $L_{sc} = 3 \times 10^{42}$ erg s^{-1}, respectively.

continuously approaching the maximum pressure until the mass of the cluster reaches the critical value M_{crit}. It was demonstrated by Tenorio-Tagle et al. (2007) that in the case without a black hole, if $M_{sc} \geq M_{crit}$, the pressure at the stagnation point, P_{st}, takes the maximum possible value and T_{st} remains equal to the value acquired at the threshold line, $T_{st} = T_{crit}$. Thus if $M_{sc} < M_{crit}$, then $T_{st} > T_{crit}$ and if

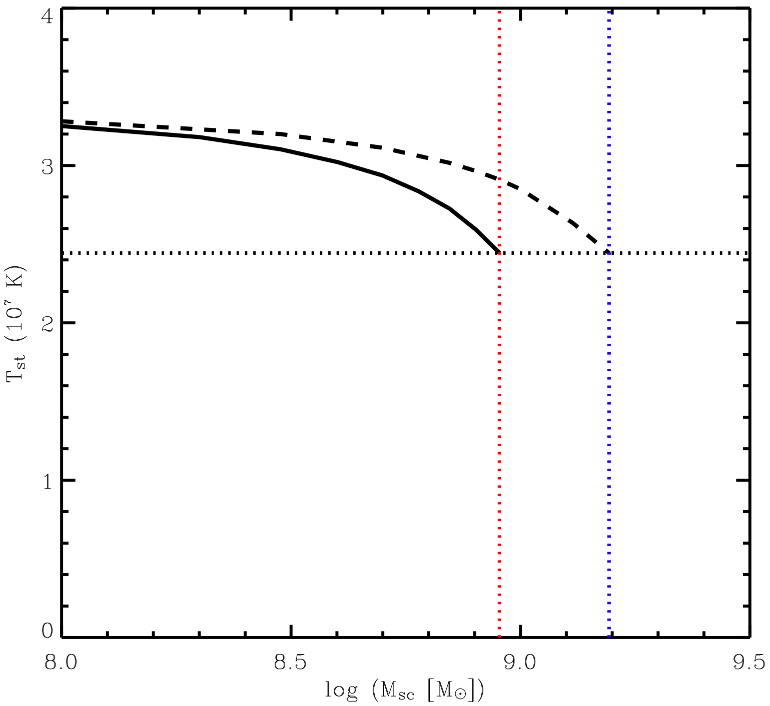

Figure 5.10: The stagnation temperature as a function of the star cluster mass. Solid line represents T_{st} in the case of the clusters with a central black hole. Dashed line shows the same in the case without the central black hole. The horizontal line represents T_{crit}. Star clusters whose masses reach the critical value are marked by the red and blue lines, in the case with and without the central black hole, respectively. The corresponding critical luminosities are $L_{crit} = 2.7 \times 10^{43}$erg s^{-1} and $L_{crit} = 4.7 \times 10^{43}$ erg s^{-1}. Note that when a central black hole is added, the threshold line shifts below the critical luminosity found in the case without a black hole. In all calculations we assumed that the mass of the BH is $10^8 M_\odot$.

$M_{sc} \geq M_{crit}$, $T_{st} = T_{crit}$ (see Figure 5.9). The vertical line in this figure marks the critical temperature and shows the track of P_{max} for clusters above the threshold energy.

The temperature at the stagnation point for 100 pc clusters with different masses and with a $10^8 M_\odot$ central BH, is shown in Figure 5.10 and is compared with the central temperature for clusters with the same radii but without BH (Figure 5.10, dashed line). As the mass of the cluster increases, T_{st}, diminishes and reaches the critical temperature, T_{crit}, (marked in Fig. 5.10 by the horizontal line) when clusters reach the critical mass, M_{crit}, (represented with red and blue vertical lines for both cases with and without BH, respectively). Note that in the BH case, M_{crit} is smaller than in the without BH case. If we look at the red line, we note that the BH shifts T_{st} to lower values for the same parameters of the cluster. Note also that when the BH is considered, T_{st} reaches the critical temperature at smaller M_{sc} value with respect to the without BH case. When $T_{st} = T_{crit}$, radiative cooling becomes a dominant factor in both cases, and the clusters evolve in the bimodal regime. In this case, R_{st} and $\dot{M}_{acc}$ are controlled by the radiative cooling of the injected matter. While below the threshold line these parameters are defined basically by the mass of the BH.

From the precedent analysis we demonstrate that in the case of low mass clusters the stagnation radius is defined by the central BH whereas for the more massive clusters - by a strong radiative cooling. One can introduce then, by analogy with the case without BH, the threshold mechanical luminosity. However in this case the threshold luminosity separates clusters whose inner structure (stagnation radius) is dominated by the central BH from that, whose stagnation radius is defined by the radiative cooling. Thus in presence of the central BH the threshold mechanical luminosity is defined by the condition

$$R_{st,BH} = R_{st,cool}, \tag{5.28}$$

where $R_{st,BH}$ and $R_{st,cool}$ are the stagnation radii required by the BH and the strong radiative cooling, respectively (see solid line in Figure 5.11). Dashed line in the same figure separates clusters for which the stagnation radius is at the center of the cluster from that, whose stagnation radius is defined by cooling.

Note that the $10^8 M_\odot$ BH used in the calculations shifts the threshold mass (luminosity) by a factor of 1.4 for the assumed $V_{A,\infty} = 1500$ km s^{-1} and $Z_\odot$.

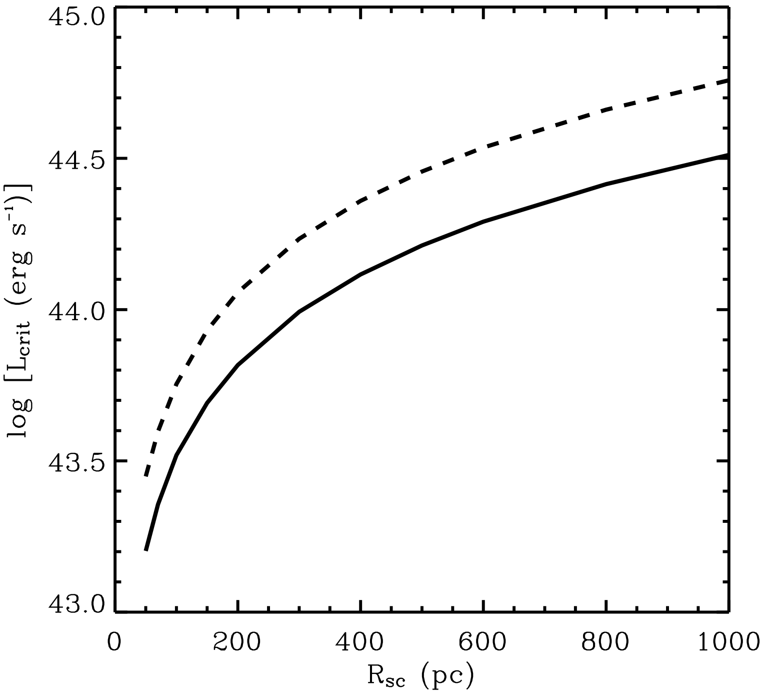

Figure 5.11: The threshold mechanical luminosity of the cluster with a central black hole. The dashed line presents the threshold luminosity for the case without the central black hole. The solid line displays the threshold luminosity for the same cluster, but with a $10^8 M_\odot$ black hole in the center. It was assumed that the adiabatic wind terminal speed is 1500 km s^{-1} and solar metallicity for the plasma.

5.6 Conclusions

In this chapter we developed a self-consistent, steady-state radiative solution for gaseous flows driven by stellar clusters with a central black hole.

We demonstrated that a black hole at the star cluster center shifts the stagnation radius from the center towards the star cluster surface. We also demonstrated that below the threshold mechanical luminosity the position of the stagnation radius is defined by two boundary conditions: the outer sonic point is at the star cluster surface and the inner one is at $r = 3R_{Schw}$. The proper solution corresponds to the minimum ρ_{st} required for a stationary solutions with positive derivatives, du/dr, across the flow.

We applied our model to the bulges of three galaxies: M32, NGC 7457 and the Milky Way, and also to the globular cluster G1 and three artificial clusters whose parameters were derived from the $M_{bulge} - M_{BH}$ relation. In spite of the fact that the bulge of the selected objects and G1 are not young starbursts we use their parameters to demonstrate that for stellar clusters below the threshold line and an arbitrary mass of the BH, our model leads always to a stationary solution.

We demonstrated that the threshold mechanical luminosity of the cluster in the case with a black hole separates clusters whose stagnation radius is defined by the BH from that, whose inner structure is defined by radiative cooling.

We propose a simple analytical approximation to the numerical accretion rate and to the position of the stagnation point (equations 5.20 and 5.26), that can be used as upper limits.

Our study is a step towards constructing a self-consistent model for spherically symmetric accretion onto the black hole at the center of a young stellar cluster (compare for example, with the isothermal model of Durisen & Burns, 1981; and the polytropic model of Bondi, 1952). The model requires some further improvements. One of them is to implement more realistic assumptions about the stellar mass distribution and to account for the radiative heating caused by radiation emerging from the accretion disc around the central black hole. However, for my future work the main problem to be addressed is the case of a central black hole inside a cluster that evolves in the catastrophic cooling regime.

Chapter 6

Conclusions of this thesis

We studied the impact of gravity on the internal structure of super stellar cluster winds. We demonstrated that the gravity field of the cluster modifies the structure of isothermal winds: in the case without gravity the gas outflow accelerates faster than in cases with gravity, because when the gravity term is neglected the central density becomes more than 4 orders of magnitude smaller than in the case with gravity. In the isothermal case without a gravity there is no critical point, and the stationary solution requires that the sonic point lies at the cluster surface. Although the isothermal assumption is simple, we have solved the problem in a self-consistent manner by taking into account the mass deposition inside the cluster.

Although the gravity force of the stellar cluster modifies the structure of the isothermal winds, here we demonstrated that the gravity field of the stellar cluster does not modify the hydrodynamic evolution of radiative winds. This results from the high pressure gradient, which exceeds the gravity force.

In order to attack the main goal of this work, we reconsidered the Bondi accretion solution as a reference for our self-consistent model. Because Bondi accretion is used in many cases, here we present a formal solution (for the accretion velocity and density distribution) in terms of dimensionless variables which can be scaled to BHs of any mass.

The main contribution of this thesis is that, we propose a solution of the spherically symmetric flows for the gas injected within super stelar clusters with a central massive black hole by using a self consistent model.

We proof that our model can be applied to AGN-SB composite with intermediate mass black holes and super massive black holes.

We demonstrated that the central BH modifies locally the behavior of the gas injected inside the stagnation point but does not change the structure of the outflow. However, from our numerical calculations, we found that the presence of the BH lowers the threshold energy below the values obtained in the cases without gravity.

We demonstrate that the threshold mechanical luminosity of young stellar clusters with a central BH separates clusters for which the stagnation radius and accretion rate is defined by the BH from that, whose inner structure is defined by radiative cooling.

In many cases, to estimate luminosities or solve accretion problems the key parameter is the mass accretion rate. As in the Bondi accretion formulation, the problem is to select the appropriate values for the density and temperature of the ISM; here we presented alternative formulae to the mass accretion rate and to the stagnation radius in terms of physical parameters of the BH and the host stellar spheroid, instead of ISM parameters.

Appendix A

Density distribution for an isothermal wind in the subsonic regime

For the subsonic region $r \leq r_c$ (the region inside the critical radius, Eq. 2.18), equation (2.12) can be written in the form

$$\frac{u}{c_s^2}\frac{du}{dr} + \frac{1}{\rho}\frac{d\rho}{dr} + \frac{GM_{sc}}{c_s^2 r^2} = 0. \tag{A.1}$$

An integration of Eq. (A.1) results in

$$\log\frac{\rho}{\rho_0} + \frac{1}{2}\left(\frac{\rho_0 u_0 r_0^2}{c_s^2 \rho r^2}\right)^2 = \frac{GM_{sc}}{c_s^2}\left(\frac{1}{r} - \frac{1}{\rho_0}\right) + \frac{u_0^2}{2c_s^2} \tag{A.2}$$

where ρ_0 and u_0 are density and velocity, respectively at a given radius r_0. Let us now compare equation (A.2) with the density distribution of a hydrostatic atmosphere. In a static atmosphere the density is given by the hydrostatic equation

$$\frac{1}{\rho}\frac{dp}{dr} + \frac{GM_{sc}}{r^2} = 0 \tag{A.3}$$

which transforms, with $p = \rho kT/\mu$, into

$$\frac{r^2}{\rho}\frac{d\rho}{dr} = -\frac{GM_{sc}}{c_s^2} \tag{A.4}$$

if the atmosphere is isothermal. The solution is

$$\log \frac{\rho}{\rho_0} = \frac{GM_{sc}}{c_s^2} \left(\frac{1}{r} - \frac{1}{r_0} \right) \tag{A.5}$$

The density structure (equation A.5) of the hydrostatic region is very similar to that of an isothermal cluster wind. In particular at the critical or sonic point where $u_0 \rho_0 r_0^2 = c_s \rho(r_c) r_c^2$, Eq. (A.2) is identical to Eq. (A.5). In fact, Eq. (A.2) remains close to Eq. (A.5) when the wind velocity is highly subsonic, $u_0 \ll c_s$. The close agreement between the hydrostatic and wind density distributions in the subsonic region is due to the fact that the term udu/dr in the momentum equation (2.12) is much smaller than the pressure gradient term.

Appendix B

l'Hopital's rule for equations with a singular point

l'Hopital's rule provides an expression for the derivative of a first order differential equation with a singular point:

$$\frac{dF}{dx} = \frac{f(x)}{g(x)}. \tag{B.1}$$

Let us suppose that this equation has a singularity at x_c, where $f(x) = 0$ and $g(x) = 0$. The derivative dF/dx at the critical point, x_c, can be found by expanding $f(x)$ and g(x) in Taylor's series around x_c.

$$\left.\frac{dF}{dx}\right|_{x_c} = \frac{f(x_c) + (x - x_c)f'(x) + \frac{1}{2}(x - x_c)^2 f''(x_c)...}{g(x_c) + (x - x_c)g'(x) + \frac{1}{2}(x - x_c)^2 g''(x_c)...} \tag{B.2}$$

If the first derivatives of f and g at x_c are both non zero then

$$\left.\frac{dF}{dx}\right|_{x_c} = \frac{f'(x_c)}{g'(x_c)}. \tag{B.3}$$

If only one of the two derivatives $f'(x_c)$ or $g'(x_c)$ is zero, then $\left.\frac{dF}{dx}\right|_{x_c}$ is either 0 or $\pm\infty$. If both $f'(x_c)$ and $g'(x_c)$ are zero, then

$$\left.\frac{dF}{dx}\right|_{x_c} = \frac{f''(x_c)}{g''(x_c)} \tag{B.4}$$

etc.

This rule is useful for determining the stationary stellar wind solution. In this case the momentum equation often has the form

$$\frac{1}{u}\frac{du}{dr} = \frac{\frac{2\gamma a^2}{r} - \frac{GM_{sc}}{r^2} + f(r)}{u^2 - \gamma a^2} \tag{B.5}$$

where $u(r)$ is the velocity, $\gamma a^2 = c_s^2$ is the square of the sound speed and function $f(r)$ represents the external forces which are different from the thermal gas pressure and gravity. The critical point occurs at r_c where the numerator and denominator are zero. At the critical point the velocity of the gas equals the sound speed

$$u^2(r_c) = c_s^2 \tag{B.6}$$

and

$$\frac{GM_{sc}}{r_c^2} - f(r_c) = \frac{2c_s^2(r_c)}{r_c} = \frac{2u^2(r_c)}{r_c} \tag{B.7}$$

The application of l'Hopital's rule to equation (B.5) in the case of isothermal wind ($\gamma = 1$ and $c_s = \ constant$) gives

$$\frac{1}{u_c}\left(\frac{du}{dr}\right)_{r_c} = \frac{-\frac{2c_s^2}{r_c^2} + \frac{2GM_{sc}}{r_c^3} + \left(\frac{df}{dr}\right)_{r_c}}{2u_c\left(\frac{du}{dr}\right)_{r_c}} \tag{B.8}$$

with $u_c = c_s$. This results in a quadratic expression for $(du/dr)_{r_c}$ whose roots are

$$\left(\frac{du}{dr}\right)_{r_c} = \pm\left[-\frac{c_s^2}{r_c^2} + \frac{GM_{sc}}{r_c^3} + \frac{1}{2}\left(\frac{df}{dr}\right)_{r_c}\right]^{1/2} \tag{B.9}$$

If we neglect df/dr, then the critical point occurs at $r_c = GM_{sc}/2c_s^2$ and

$$\left(\frac{du}{dr}\right)_{r_c} = \pm\frac{2c_s^3}{GM_{sc}} \tag{B.10}$$

For a wind with an outward increasing velocity the positive sign in (B.10) must be adopted. The determination of the velocity gradient in the critical point by l'Hopital's rule is essential for the numerical integration of the momentum equation because it allows a smooth transition through a region where the numerical integration is impossible because du/dr is uncertain.

Appendix C

The Bondi accretion rate for the cases $\gamma = 5/3$ and $\gamma = 1$

The Bondi accretion rate is defined by the gas parameters far away from the center:

$$\dot{M} = \pi G^2 M^2 \frac{\rho_{ISM}}{c_{ISM}^3} \left(\frac{2}{5-3\gamma}\right)^{\frac{5-3\gamma}{2(\gamma-1)}}. \tag{C.1}$$

In the adiabatic case ($\gamma = 5/3$) the factor

$$f = \left(\frac{2}{5-3\gamma}\right)^{\frac{5-3\gamma}{2(\gamma-1)}} \tag{C.2}$$

is uncertain. One can avoid this problem taking the logarithm, from both sides of equation (C.2) and then apply l'Hopital's rule to the resulting expression:

$$\log f = \frac{5-3\gamma}{2(\gamma-1)} \log\left(\frac{2}{5-3\gamma}\right). \tag{C.3}$$

Note that (C.3) has the form

$$\log f = \frac{1}{\gamma-1} \frac{\log x}{x}, \tag{C.4}$$

where $x = 2/(5-3\gamma)$. When $\gamma \to 5/3$, the $\log x/x$ has the undetermined form ∞/∞. l'Hopital's then gives

$$lim_{x\to\infty} \frac{\log x}{x} = lim_{x\to} \frac{\frac{1}{x}}{1} = 0. \tag{C.5}$$

Therefore $\log f(5/3)$=0 that implies that $f = 1$. So the accretion rate is

$$\dot{M} = \pi G^2 M^2 \frac{\rho_{ISM}}{c_{ISM}^3}. \tag{C.6}$$

In the isothermal case ($\gamma = 1$), equation (C.3) can be expressed as

$$\log f = \frac{5 - 3\gamma}{2(\gamma - 1)}[\log 2 - \log(5 - 3\gamma)] \tag{C.7}$$

which has the form 0/0 for $\gamma = 1$. If $g = [(5-3\gamma)/2][\log 2 - \log(5-3\gamma)]$ and $h = \gamma - 1$, its derivatives are $g' = 3/2$ and $h' = 1$, respectively. And l'Hopital's rule gives

$$\log f = \frac{g'}{h'} = \frac{3}{2}, \quad \text{then} \quad f = e^{3/2}. \tag{C.8}$$

Therefore, the accretion rate is

$$\dot{M} = \pi G^2 M^2 \frac{\rho_{ISM}}{c_{ISM}^3} e^{3/2}. \tag{C.9}$$

Appendix D

The relation between the gas density and temperature at the stagnation point

The relation between the gas number density and temperature at the stagnation point can be found from the energy and mass conservation equations:

$$\frac{du}{dr} = \frac{1}{\rho}\frac{(\gamma-1)(q_e-Q)+q_m\left[\frac{(\gamma+1)}{2}u^2-\frac{2}{3}\left(1-\frac{R_{st}^3}{r^3}\right)\left(c_s^2-\frac{V_e^2}{4}\right)\right]}{c_s^2-u^2}, \tag{D.1}$$

$$\rho u r^2 = \frac{q_m r^3}{3}\left(1-\frac{R_{st}^3}{r^3}\right). \tag{D.2}$$

An evaluation of the equation (D.1) at the stagnation point ($u = 0$), results in

$$\left.\frac{du}{dr}\right|_{r=R_{st}} = \frac{(\gamma-1)(q_e-Q)}{\rho c_s^2}. \tag{D.3}$$

The derivative of the velocity from equation (D.2) is

$$\frac{du}{dr} = \frac{q_m}{3\rho}\left[1+\frac{2R_{st}^3}{r^3}+\frac{1}{\rho}\left(\frac{R_{st}^3}{r^2}-r\right)\right]. \tag{D.4}$$

At $r = R_{st}$, it is

$$\left.\frac{du}{dr}\right|_{r=R_{st}} = \frac{q_m}{\rho_{st}}. \tag{D.5}$$

The comparison of equations (D.3) and (D.5) then results in

$$n_{st} = q_m^{1/2} \left[\frac{q_e/q_m - c_{st}^2/(\gamma - 1)}{\Lambda(Z, T_{st})} \right]^{1/2} \tag{D.6}$$

Thus, the relation between the gas number density and the temperature at the stagnation point remains the same as derived by Silich et al. (2004) for the case without gravity.

List of Tables

List of Figures

References

Barth, A. J., Greene, J. E., & Ho, L. C. 2005, ApJ, 619, L151

Baum, S. A., O'Dea, C. P., Dallacasa, de Bruyn, A. G. & Pedlar, A. ApJ, 419, 553

Baumgardt, H., Makino, J., Hut, P., McMillan, S., & Portegies Zwart, S. 2003, ApJ, 589, L25

Bissantz, N., Englmainer, P., Binney, J., & Gerhard, O. 1997, MNRAS, 289, 651

Blandford, R. D., & Begelman, M. C. 1999, MNRAS, 303, L1

Bondi, H., & Hoyle, F. 1944, MNRAS, 273

Bondi, H. 1952, MNRAS, 112, 195

Cantó, J., Raga, A. C., & Rodriguez, L. F. 2000, ApJ, 536, 896

Chevalier, R. A., & Clegg, A. W. 1985, Nature, 317, 44

Di Mateo, T., Allen, S. W., Fabian, A. C., & Wilson, A. S. 2003, ApJ, 582, 133

Durisen, R. H., & Burns, J. O. 1981, MNRAS, 195, 535

Ferrarese, L., & Merritt, D. 2000, ApJ, 539, L9

Ford, H. C., et al. 1995, ApJ, 1994, 435, L27

Frank, J., King, A., & Raine, D. Accretion Power in Astrophysics, Cambridge University Press, Third Edition, 2002

Freedman, W. L., et al. 2001, ApJ, 553, 47

Gebhardt, K., et al. 2000, ApJ, 539, L13

Gebhardt, K., Rich, R. M., & Ho, L. C. 2002, 578, L41

Gebhardt, K., et al. 2003, ApJ, 583, 92

Gebhardt, K., Rich, R. M., & Ho, L. C. 2005, 634, 1093

Gerhard, O. 2000, in Lançon A., Boily C. M., eds., ASP Conf. Ser. Vol. 211, Massive Stellar Clusters. Astron. Soc. Pac., San Francisco p. 12

González Delgado, R. M., Heckman, T., Litherer, C., Meurer, G., Krolik, J., Wilson, A. S., Kinney, A. & Koratkar, A. 1998, ApJ, 505, 174

Greene, J. E., & Ho, L. C. 2006, ApJ, 641, L21

Harms, R. J., et al. 1994, ApJ, 435, L35

Häring, N., & Rix, H. W. 2004, ApJ, 604, L89

Heckman, T., González Delgado, R. M., Litherer, C., Meurer, G., Krolik, J., Wilson, A. S., Koratkar, A. & Kinney, A. 1997, ApJ, 482, 114

Holzer, T. E., & Axford, W. I. 1970, ARA&A, 8, 31

Jiménez-Bailón, E., Santos-Lleó, M., Dalhem, M., Mas-Hesse, J. M., Guainazzi, M., Heckman, T. M. & Weaver, K. A. 2005, A&A, 442, 861

Lamers, H. J. G. M., & Cassinelli, J. P. Introduction to Stellar Winds, Cambridge University Press, First Edition, 1999

Leitherer, C., & Heckman, T. M. 1995, ApJS, 96, 9

Leitherer, C., et al. 1999, ApJS, 123, 3

Lípari. S. L., & Terlevich, R. J. 2006, MNRAS, 368, 1001

Levenson, N. A. Weaver, K. A. & Heckman, T. M. 2001, ApJ, 550, 230

Macchetto, F., Marconi, A., Axon, D. J., Capetti, A., Sparks, W., & Crane, P. 1997, ApJ, 489, 579

Magorrian, J., et al. 1998, AJ, 115, 2285

Marconi, A., & Hunt, L. K. 2003, ApJ, 589, L21

Merritt, D., & Ferrarese, L. 2001, ApJ, 547, 140

Meyland, G., Sarajedini, A., Jablonka, P., Djorgovski, S. G., Bridges, T., & Rich, R. M. 2001, AJ, 122, 830

Pooley, D., & Rappaport, S. 2006, ApJ, 644, L45

Raga, A. C., Velázquez, P. F., Cantó, J., Masciadri, E., & Rodriguez, L. F. 2001, ApJ, 559, L33

Raymond, J. C., Cox, D. P., & Smith, B. W. 1976, ApJ, 204, 290

Raymond, J. C. & Smith, B. W. 1977, ApJS, 35, 419

Rodríguez Espinosa, J. M., Rudy, R. J. & Jones, B. ApJ, 312, 555

Rodríguez, G. A. 2006, PhD thesis, Instituto Nacional de Astrofísica Óptica y Electrónica, Tonantzintla, Puebla, México 72000

Rupke, D. S., Veilleux, S. & Sanders, D.B. 2005, ApJ, 632, 751

Sarazin, C. L., & White, III, R. E. 1987, ApJ, 320, 32

Schödel, R., et al. 2002, Nature, 419, 694

Silich, S., Tenorio-Tagle, G., Rodríguez-Gonález, A. 2004, ApJ, 610, 226

Smith, L. J., & Gallagher, III. J. S. 2001, MNRAS, 000, 1

Stone, J. M., Pringle, J. E., & Begelman, M. C. 1999, MNRAS, 310, 1002

Strömgren, B. 1939, ApJ, 89, 526

Sutherland, R. S., & Dopita, M. A. 1993, ApJS, 88, 253

Tenorio-Tagle, G., Wünsch, R., Silich, S., & Palouš, J. 2007, ApJ, 658, 1196

Tremaine, S., et al. 2002, ApJ, 574, 740

Verolme, E. K., et al. 2002, MNRAS, 335, 517

Wünsch, R., Palouš, J., Tenorio-Tagle, G., & Silich, S. 2007, in IAU Symposium, Vol. 237, IAU Symposium, 497-497